[redacted]

CYCLOTRON RESEARCH

UNIVERSITY OF WASHINGTON

ANNUAL PROGRESS REPORT 1964

U. S. ATOMIC ENERGY COMMISSION
CONTRACT A.T. (45-1)-1388

UNIVERSITY OF WASHINGTON

Department of Physics

Cyclotron Research

PROGRESS REPORT FOR YEAR ENDING JUNE 15, 1964

PROGRAM "A"--EXPERIMENTAL NUCLEAR PHYSICS PROGRAM (CYCLOTRON)

UNDER

U.S. ATOMIC ENERGY COMMISSION CONTRACT A.T. (45-1)-1388

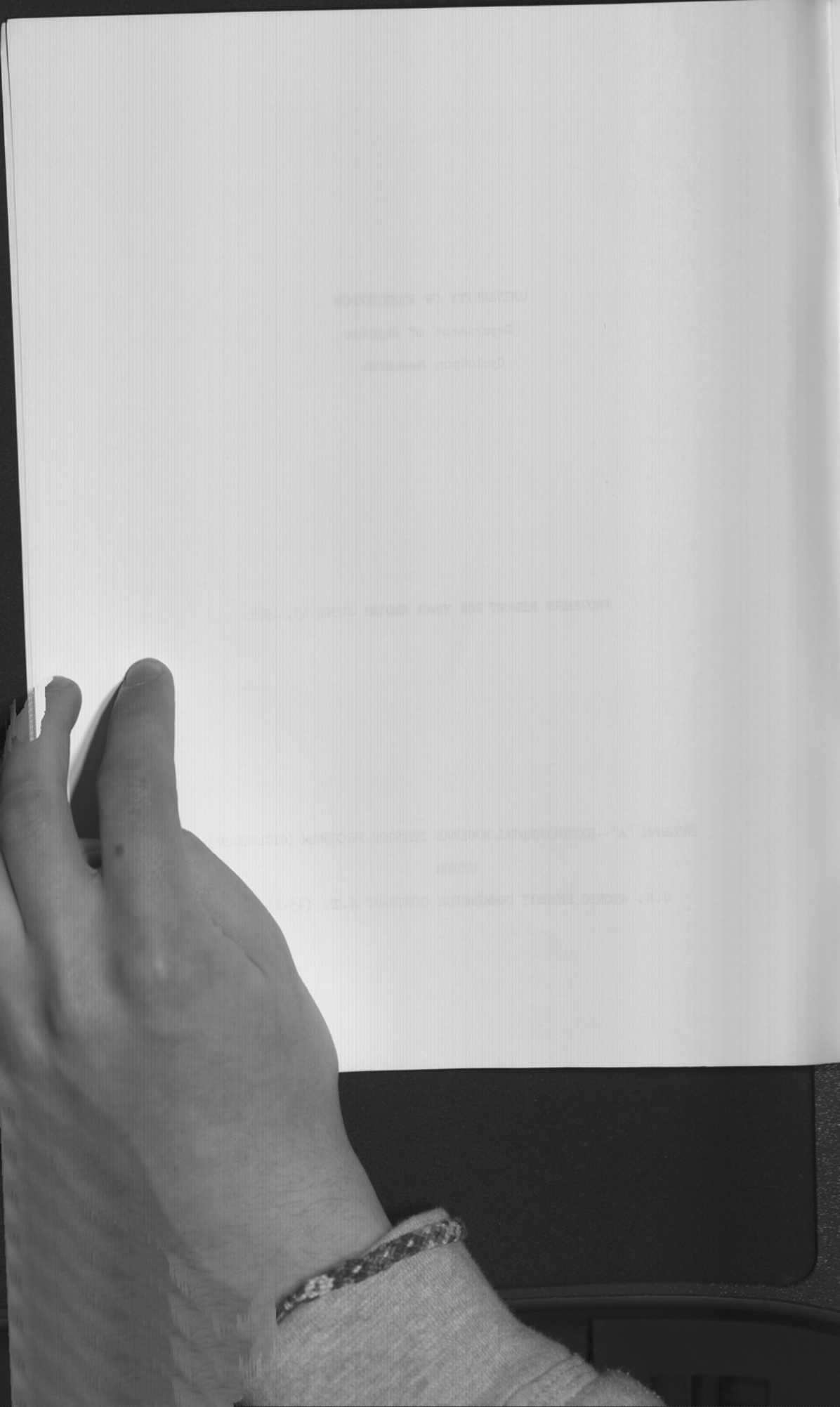

PREFACE

This report reviews the research and technical development conducted at the Nuclear Physics Laboratory of the University of Washington during the year ending June 15, 1964.

Research at this laboratory is performed by the faculty and graduate students of the Departments of Physics and Chemistry of the University of Washington. Support for this project is provided by the State of Washington, the U.S. Atomic Energy Commission, and the National Science Foundation.*

The arrangement of this report follows the pattern used in previous years. The sections are numbered consecutively through the report; each table and figure is assigned the number of the section to which it pertains. As has been our practice, the names of investigators listed at the end of each section are given in strict alphabetical order.

The investigations described in this report for the most part continue and extend experimental work described in several earlier reports. Continued emphasis has been placed on inelastic scattering, including alpha-gamma and proton-gamma angular correlations. Inelastic scattering to the continuum as well as to discrete states is under investigation. Other studies include pickup reactions, particles and gamma rays emitted by compound nuclei, fission, and light-element capture and breakup reactions. An increasing amount of effort is going into planning and development of instrumentation for the new tandem.

A highlight of the past year has been completion of the new building which will house the tandem Van de Graaff and also provides much-needed additional laboratory space. This building was occupied this spring, and installation of the new accelerator will commence in early summer.

---

*The National Science Foundation has provided funds for the purchase of the Van de Graaff accelerator and some of its associated equipment and, in part, for the building to house the new accelerator.

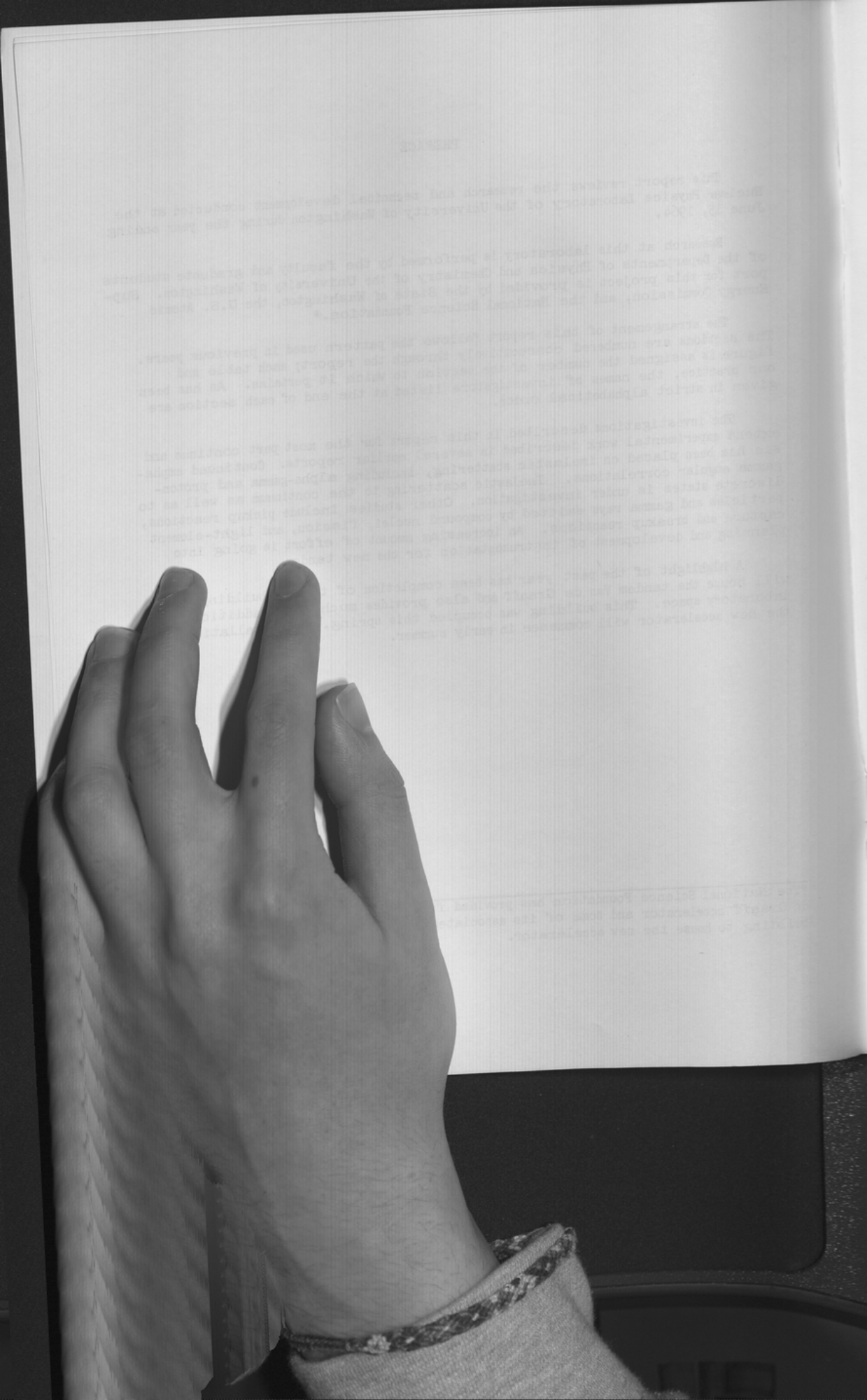

TABLE OF CONTENTS

I. BETA AND GAMMA RAY SPECTROSCOPY

1. 4.1 MeV Positron Spectrum of O^{14}

The experiment to determine the shape of the Gamow-Teller branch of the O^{14} positron spectrum, mentioned in earlier reports,[1] was interrupted by the plugging of the solenoidal beta-ray spectrometer coils and their reconstruction. The capability of the new coils for carrying much larger currents without overheating and the consequent extended range of the spectrometer (see Section 33) will permit the comparatively long counting times required because of low counting rates of the high energy positrons. To avoid the large distortion caused by backscattering of beta particles from the thick copper rod, mentioned in the last report,[2] different methods of trapping the O^{14} activity are being explored. A deposit of $CaCl_2$ pressed in a hydraulic press and glued to mylar has proved the most satisfactory catcher for trapping the H_2O^{14} activity. Attempts to make still thinner samples of uniform thickness to minimize backscattering are in progress.

An alternative method using Be backing instead of a cooled copper rod should reduce backscattering to a negligible value. The attempts so far with this backing are not conclusive.

A new beta-ray counter has been built and installed for use as a detector for the spectrometer. Its construction is similar to the gamma-ray monitor counter built in 1962,[3] but with a five-foot-long light pipe and an exposed plastic scintillator. The motive for this was to discriminate against the gamma-ray background and to avoid deadtime corrections, both of which were excessive with the G.M. counter used in the past. (J. B. Gerhart and G. S. Sidhu)

---

1 Cyclotron Research, University of Washington (1963), p. 1; (1962), p. 2; (1961), p. 2; (1959), p. 5.

2 Cyclotron Research, University of Washington (1963), p. 1.

3 Cyclotron Research, University of Washington (1962), p. 54.

II. ELASTIC AND INELASTIC SCATTERING ANGULAR DISTRIBUTIONS

2. Alpha Particle Scattering from Li^7

A study has been made of the differential cross sections for the elastic and inelastic scattering of 42 MeV alpha particles by Li^7. Our attention has been directed to this nucleus by recent applications[1 - 5] of collective models tc Li^7 and nearby nuclei in the middle of the p shell. Further, our interest has been stimulated by an experimental study[6] of inelastic scattering of high energy electrons from this nucleus.

Targets were prepared by evaporating natural lithium (93% Li^7) onto thin nylon backings. The evaporator was let down to an inert gas, and the target was rushed to a similarly filled scattering chamber.

Since the kinematic broadening of the scattered alpha particles is as high as 450 keV/degree at 45°, it was necessary that the angular acceptance of the solid state detector be kept very small. In this manner the widths of all experimental peaks were held below 200 keV, and the levels of Li^7 could be found readily among the impurity peaks as is indicated by the experimental spectrum shown in Figure 2-1.

The experimental angular distributions for elastic and inelastic scattering are shown in Figure 2 - 2. An uncertainty in determining the target thickness has precluded assignment of absolute cross sections at the present time.

We discuss these data first in terms of the following general considerations. For an odd nucleon strongly coupled to a permanently deformed core, the adiabatic approximation for the scattering predicts that the elastic and inelastic cross-sections should be given by:

$$d\sigma/d\Omega \Big|_{\text{elastic}} = d\sigma/d\Omega \Big|_{0^+} + (I_i 2K0 \,|\, I_i K)^2 \; d\sigma/d\Omega \Big|_{2^+}$$

$$d\sigma/d\Omega \Big|_{\text{inelastic}} = (I_i 2K0 \,|\, I_f K)^2 \; d\sigma/d\Omega \Big|_{2^+}$$

where $d\sigma/d\Omega \,|_{0^+}$ is the elastic cross-section for an even nucleus of the same radius and deformation as the odd, and $d\sigma/d\Omega \,|_{2^+}$ is the corresponding cross-section to the first rotational state. The Clebsch-Gordan coefficients come from coupling the odd nucleon to the rotating core. I_i and I_f are the initial and final spins, and K is the projection of the angular momentum along the axis of symmetry. According to this, the inelastic cross-sections to the members of the K = 1/2 ground state rotational band (Figure 2-3) would be in the ratio:

$$1/2 : 7/2 : 5/2 = 1/5 : 18/35 : 3/35$$

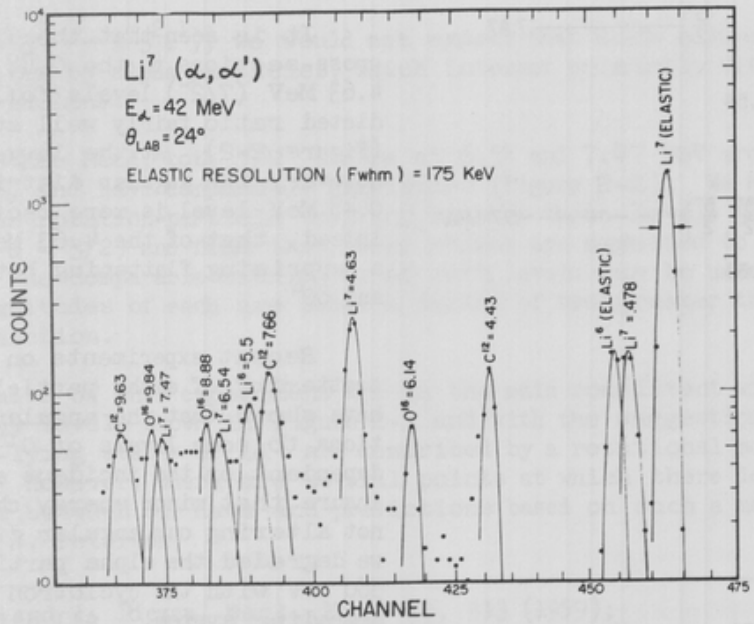

Fig. 2-1 Pulse height spectrum at 24° of 42 MeV alpha particles scattered from natural lithium evaporated onto nylon. The greater widths of the 4.63, 6.54, and 7.47 MeV levels are seen.

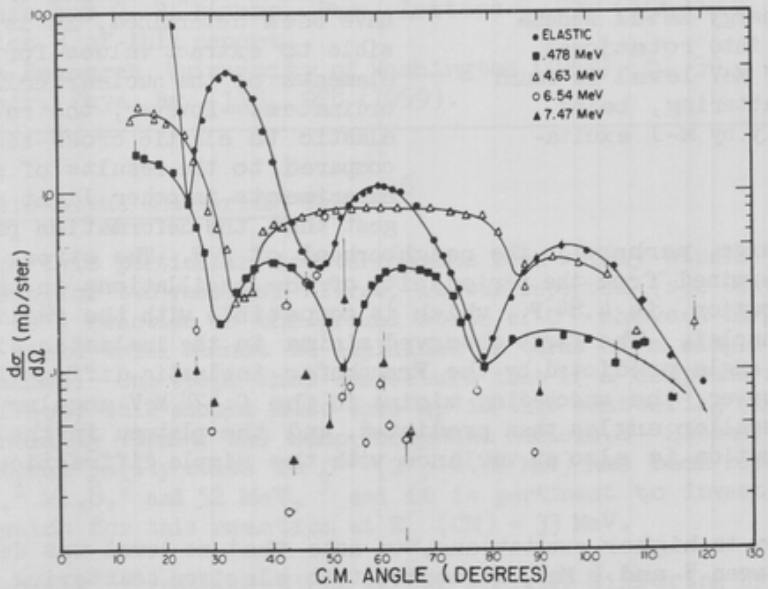

Fig. 2-2 Differential cross sections for alpha particles scattered from Li^7. Error bars are relative only. There is approximately 10% uncertainty in the over-all absolute cross section.

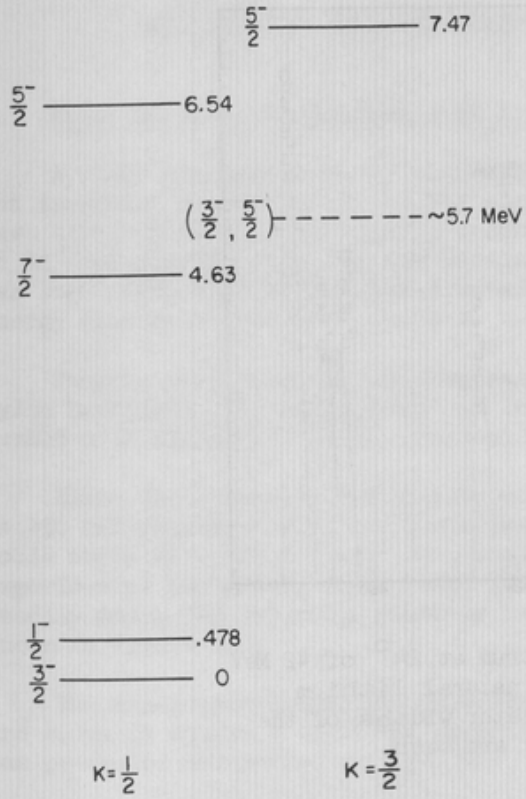

Fig. 2-3 Energy level scheme of Li^7, broken into rotational bands. The 5.7 MeV level is found by electron scattering, being populated mainly by M-1 excitation.

It is seen that the differential cross-sections to the 0.48 MeV ($1/2^-$) and 4.63 MeV ($7/2^-$) levels follow the predicted ratio fairly well at small angles (Figure 2-2). At the larger angles, however, the angular distribution of the 0.48 MeV level is more oscillatory and, indeed, that of the 4.63 MeV level shows a surprising flattening between $\theta = 40^\circ$ and 80°.

Recent experiments on the inelastic scattering of alpha particles on O^{16} [7] have shown that the angular distributions to some levels of O^{16} are strongly dependent on the incident energy. To insure that minor energy changes were not altering our angular distributions, we degraded the alpha particle beam by 580 keV with the cyclotron beam energy degrading system.[8] All differential cross sections remained unchanged, and, in particular, the plateau in the angular distribution to the 4.63 MeV level is unaltered.

Since only relative cross sections have been determined, it is not yet possible to extract values for the matrix elements of the nuclear collective coordinates. However, the ratios of inelastic to elastic cross-sections, when compared to the results of similar experiments in other light nuclei, suggest that the deformation parameter, $\delta_2 = \beta_2 R$, is large, perhaps in the neighborhood of 2 F. The strong absorbtion radius, R, determined from the periodicity of the oscillations in the elastic angular distribution, is 4.84 F., which is compatible with the radii found in other p-shell nuclei. The first observed minima in the inelastic distributions occur near the angle predicted by the Fraunhofer inelastic diffraction scattering model[9]; however, the succeeding minima in the 0.478 MeV angular distribution occur at smaller angles than predicted, and the plateau in the 4.63 MeV angular distribution is also at variance with the simple diffraction model.

Turning now to higher excitations, we note that no level was detected for excitations between 5 and 6 MeV, in contrast to electron scattering experiments,[6] which suggest a level at 5.7 MeV with spin $3/2^-$ or $5/2^-$, populated mainly by M-1 excitation. Additional evidence for this state is scanty. (See Reference 5 for a summary of the data.) Since excitation of this level is presumed to correspond to a single particle change in the intrinsic nuclear

structure ($1^4 3^3 \rightarrow 1^4 3^2 2^1$), we would not expect that such a level would be strongly excited by alpha particles, which interact primarily with collective modes of the nucleus.

On the other hand, both $5/2^-$ states at 6.54 and 7.47 MeV are excited, albeit weakly, and have comparable magnitudes (Figure 2-2). We have made calculations of the rotation-particle coupling between these levels (J = 5/2, K = 1/2 and J = 5/2, K = 3/2) and find that these states are expected to be very strongly mixed. Thus the comparable excitation of both levels can be understood. However, the magnitudes of each are about a factor of two greater than the strong coupling prediction.

The results of this experiment are in the main consistent with the assignment of energy levels shown in Figure 2-3 and with the suggestion of Reference 5, that the low-lying states of Li^7 are described by a rotational model with interband mixing. However, there are several points at which there do seem to be discrepancies between our data and predictions based on such a model. (J.S. Blair and R. J. Peterson)

---

1 D. Kurath and L. Picman, Nucl. Phys. 10, 313 (1959);
D. Kurath, Phys. Rev. 101, 216 (1956).
2 A. B. Clegg, Phil. Mag. 6, 1207 (1961);
A. B. Clegg, Nucl. Phys. 33, 194 (1962).
3 J. S. Blair and E. M. Henley, Phys. Rev. 112, 2029 (1958).
4 P. D. Kunz, Ann. of Phys. 11, 275 (1960).
5 C. M. Chesterfield and B. M. Spicer, Nucl. Phys. 41, 675 (1963).
6 M. Bernheim and G. R. Bishop, Phys. Letters 5, 294 (1963).
7 See Section 3 of this report.
8 Cyclotron Research, University of Washington (1963), p. 30.
9 J. S. Blair, Phys. Rev. 115, 928 (1959).

---

3. Inelastic Alpha Scattering from O^{16}

Although this particular scattering has been widely studied, we have done the experiment for two reasons: First, it was reported (see Section 15) that the O^{16} (α, Be^8) reaction to the ground state of C^{12} shows a large energy variation in Be^8 yield which cannot be explained in terms of a simple direct interaction mechanism. One would thus conjecture that if a compound nuclear component is in effect, this should also show up in this scattering experiment since we are essentially forming the same "compound nucleus." Second, the excitation of the unnatural parity state in O^{16} (2^-, 8.88 MeV) has been reported at E_α (CM) = 14.7,[1] 21.8,[2] and 52 MeV,[3] and it is pertinent to investigate the angular distribution for this reaction at E_α (CM) = 33 MeV.

Measurements of cross-sections at two energies differing by 1.2 MeV (41.2 and 40.0 MeV) were made using as a target commercially available oxygen gas (approximately 99.7% O^{16}) contained in a thin-walled cylinder[4] at a pressure of about 2 atmosphere. The scattered α-particles were detected by a RCA silicon-junction solid state detector capable of stopping 42 MeV α-particles.

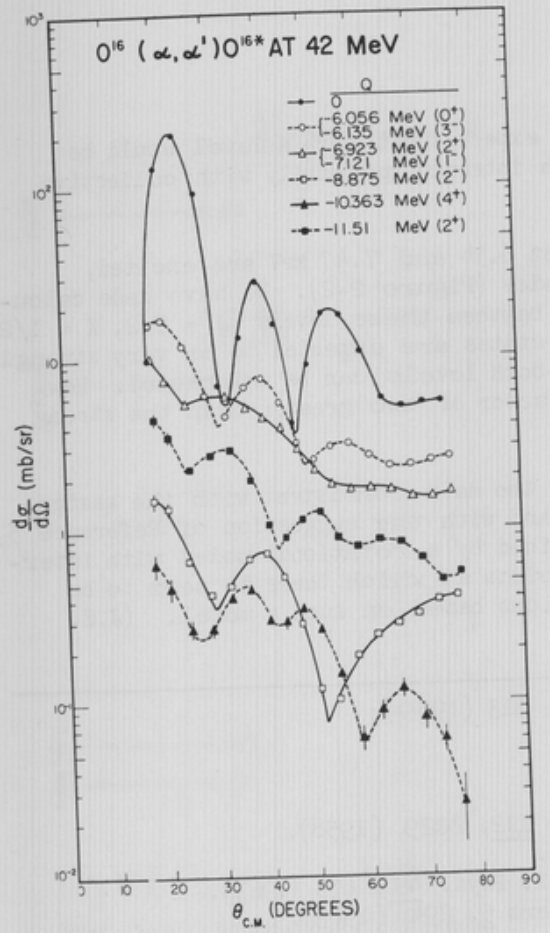

Fig. 3-1 Center-of-mass cross section for $O^{16}(\alpha,\alpha')O^{16*}$ at 41.2 MeV (nominal) incident energy. Only statistical errors are indicated.

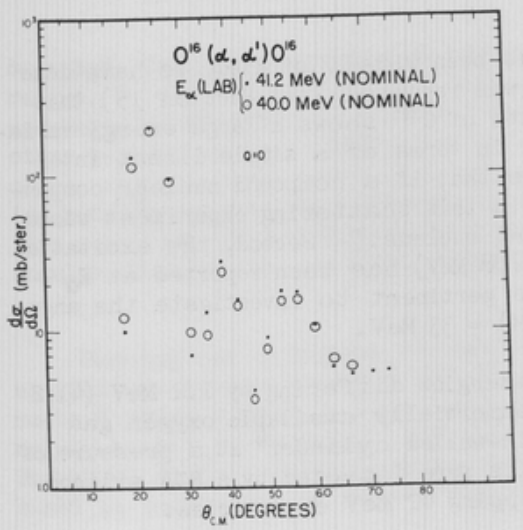

The angular distributions at 41.2 MeV incident energy are shown in Figure 3-1.

The doublet at 6.14 MeV (3^-) is not resolved, but the contributions of the 0^+ level cannot be large since the Blair phase rule for an odd-parity transition is followed. The doublet at 7.0 MeV is also not resolved and results are plotted as the sum of the two contributions.

The 8.88 MeV (2^-) cross section is seen to oscillate about 1-1/2 times the period of the elastic distribution as compared with the results at E_α(CM) = 14.7,[1] 21.8,[2] and 52 MeV[3] which give a period of $\sim 1/2$, ~ 1, and $\sim$ 1-1/2 times the elastic period respectively. The averaged cross section decreases monotonically with increasing energy, i.e., 2.5.[1] 1.3,[2] 0.5 and 0.2 mb/sr[3] in that order. As was first pointed out by Eidson and Cramer,[5] this is in a reverse direction from the results of calculations based on a spin-orbit interaction for the reaction mechanism. A spin-orbit interaction is one of several possible mechanisms for excitation of states with unnatural parity.

The only other levels that are sufficiently excited and adequately resolved are the 10.36-MeV (4^+) and 11.51-MeV (2^+) levels; the corresponding cross sections are plotted in Figure 3-1. The Blair phase rule is seen to be approximately followed.

Fig. 3-2 Center-of-mass cross section for $O^{16}(\alpha,\alpha')O^{16*}$, Q = 0 at 40.0 MeV and 41.2 MeV incident energies.

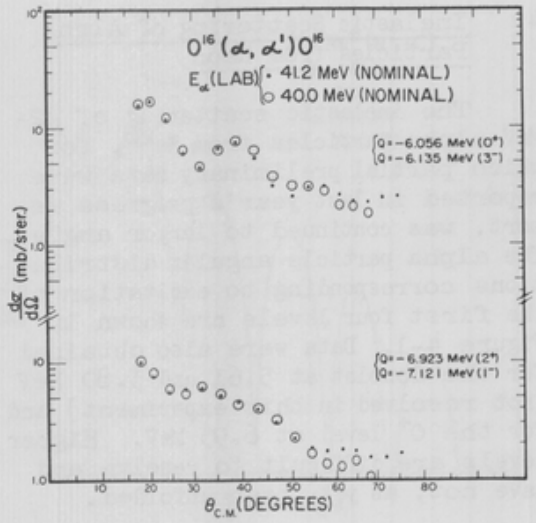

Fig. 3-3 Center-of-mass cross section for O^{16} $(\alpha,\alpha')O^{16*}$, Q = -6.14 and -7.0 MeV at 40.0 MeV and 41.2 MeV incident energies.

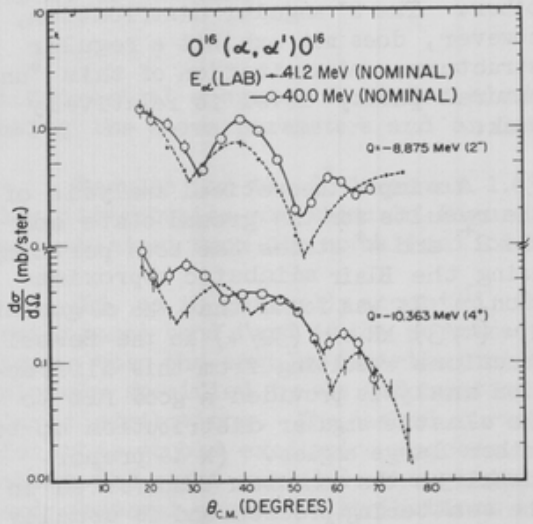

Fig. 3-4 Center-of-mass cross section for O^{16} $(\alpha,\alpha')O^{16*}$, Q = -8.80 and -10.36 MeV at 40.0 MeV and 41.2 MeV incident energies. Only statistical errors are indicated.

Figures 3-2, 3-3, and 3-4 provide comparisons of the angular distributions at two incident energies. It is seen that the elastic (Figure 3-2) and the 6.14 MeV level and the doublet at 7.0 MeV (Figure 3-3) show essentially identical results between 17° and 50° (CM).

On the other hand, the 8.88- and 10.36-MeV levels show a definite variation with energy, and the 10.36-MeV level shows a striking change of phase. Moreover, the integrated partial cross sections from 18° to 70° have increased from 92.4 mb (8.88 MeV) and 54.0 mb (10.36 MeV) at 41.2 MeV to 125.0 mb and 70.4 mb respectively at 40.0 MeV. The energy variations observed in the inelastic scattering to some of these levels may indicate some compound nuclear contribution to the scattering process. (R. E. Brown, N. Cue, and D. Shreve)

1 J. C. Corelli, E. Bleuler, and D. J. Tendam, Phys. Rev. 116, 1184 (1959).

2 J. Kokame, K. Fukunaga, N. Inoue, and H. Nakamura, Phys. Lett. 8, 342 (1964).

3 B. G. Harvey, E. J-M. Rivet, A. Springer, J. R. Meriwether, W. B. Jones, J. H. Elliott, and P. Darriulat, E. O. Lawrence Radiation Laboratory, University of California Report No. UCRL-10727 Rev. (1963).

4 Cyclotron Progress Report, University of Washington (1963), Section 28.

5 W. W. Eidson and J. G. Cramer, Phys. Rev. Lett. 9, 497 (1962).

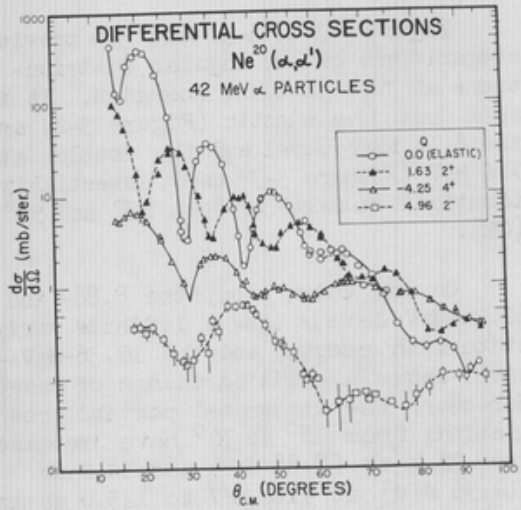

Fig. 4-1 Differential cross sections for scattered alpha particles corresponding to the lowest four levels in Ne^{20}.

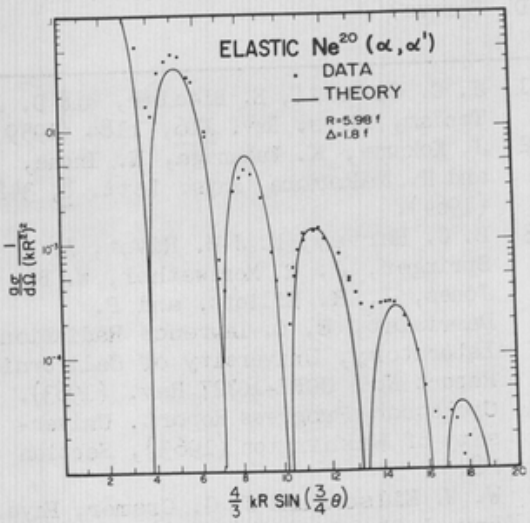

Fig. 4-2 Comparison of experimental angular distribution with Blair smoothed cut-off approximation for the elastic scattering of 42 MeV alpha particles from Ne^{20}.

4. Inelastic Scattering of Alpha Particles from Neon

The inelastic scattering of 42-MeV alpha particles from Ne^{20}, for which partial preliminary data were reported in last year's progress report, was continued to larger angles. The alpha particle angular distributions corresponding to excitation of the first four levels are shown in Figure 4-1. Data were also obtained for the doublet at 5.61 and 5.80 MeV (not resolved in this experiment) and for the 0^+ level at 6.95 MeV. Higher levels are difficult to resolve and have not, as yet, been unfolded.

Angular distributions for the ground state (elastic scattering), the 2^+ level, and the 4^+ level show the diffraction-like structure usually observed for such reactions; a point of interest is that the 2^+ and 4^+ distributions are out of phase with each other. The 2^- angular distribution, however, does not exhibit a regular structure, and excitation of this "unnatural parity" level is relatively weak.

A simple theoretical analysis of the results for the ground state and the 2^+ and 4^+ states has been performed using the Blair adiabatic approximation.[1] It was found that the argument $x = (4/3)\ kR \sin(3\theta/4)$ in the Bessel functions resulting from this diffraction analysis provided a good fit to the elastic angular distribution up to rather large angles. (x is proportional to the momentum transferred in the scattering process and is usually taken as $kR\theta$ or $2kR \sin\theta/2$, depending on the choice of shadow plane in the diffraction analysis.) The analysis included a transition effect based on an effective surface thickness of 1.8 F; this provides reduced cross sections (relative to the sharp cut-off predictions) at large angles, in agreement with the experimental results. These same parameters (momentum transfer and surface thickness) were used in the theoretical curves for the 2^+ and 4^+ angular distributions. Figure 4-2 compares the observed

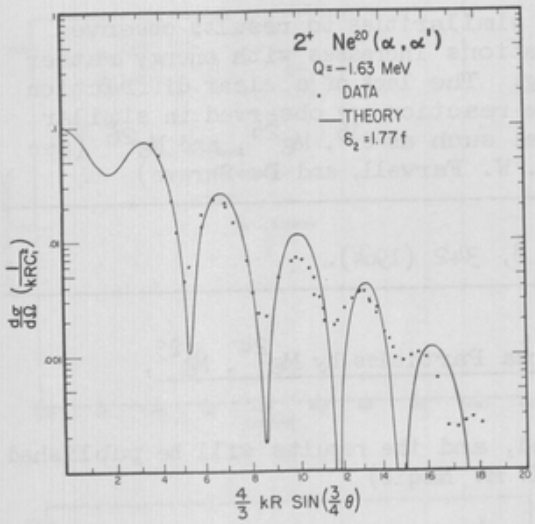

Fig. 4-3 Comparison of experimental angular distribution with Blair smoothed cut-off adiabatic approximation for the inelastic scattering of 42-MeV alpha particles from Ne^{20}. The 1.63 MeV (2^+) level is excited.

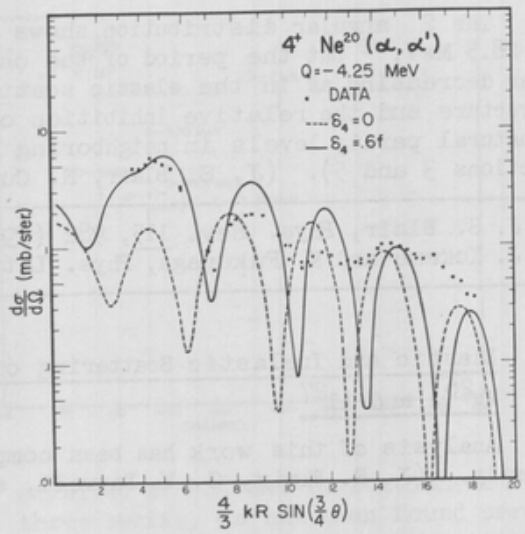

Fig. 4-4 Comparison of experimental angular distribution with Blair smoothed cut-off adiabatic approximation (the full curve includes a contribution from a 2^4-pole deformation) for the inelastic scattering of 42 MeV alpha from Ne^{20}. The 4.25 MeV (4^+) level is excited.

differential cross sections for elastic scattering with the results predicted using the above parameters and an interaction radius R = 5.98 F.

Results for the 2^+ level at 1.63 MeV and the corresponding predicted angular distribution are shown in Figure 4-3. A quadrupole deformation, δ_2 = 1.764 F was obtained from the normalization of the theoretical curve to the data.

If, as is generally accepted, the 4^+ level is a member of the ground state rotational band, and if the permanent deformation is wholly of the quadrupole type, then the angular distribution for excitation of this level should be completely specified by the information obtained from the ground state and 2^+ angular distributions. The dashed curve in Figure 4-4 gives the results expected for this double excitation process. Predicted cross sections are seen to be of about the right magnitude though too small at small angles, and the predicted and observed angular distributions are slightly out of phase. The possible effect of a 2^4 pole deformation (either permanent or vibrational) has been considered; such a deformation would contribute to the cross-section in the first order, while the quadrupole deformation contributes in second order. The solid curve in Figure 4-4 shows the result of adding a 2^4 pole deformation, δ_4 = 0.5 E. This curve is seen to agree with the data at small angles and to provide reasonable agreement with respect to phase. The lack of sharp structure in the observed angular distribution suggests that such interference may in fact be taking place, and it would be interesting to see what happens with this type of analysis in distorted wave calculations.

The 2^- angular distribution shows some similarities to results observed at 28.5 MeV, [2] but the period of the oscillations increases with energy rather than decreasing as in the elastic scattering. The lack of a clear diffraction structure and the relative inhibition of the reaction are observed in similar unnatural parity levels in neighboring nuclei such as O^{16}, Mg^{24}, and Mg^{26} (see Sections 3 and 5). (J. S. Blair, N. Cue, G. W. Farwell, and D. Shreve)

1 J. S. Blair, Phys. Rev. 115, 982 (1959).
2 J. Kokame and K. Fukunaga, Phys. Letters 8, 342 (1964).

5. Elastic and Inelastic Scattering of Alpha Particles by Mg^{24}, Mg^{25}, Mg^{26}, and Al^{27}

Analysis of this work has been completed, and the results will be published shortly. (J. S. Blair, G. W. Farwell, and I. M. Naqib)

6. Inelastic Scattering of 42-MeV α-Particles from Pb^{207}, Pb^{208}, and Bi^{209}

The study of the inelastic scattering of α-particles from nuclei in the lead region was undertaken partly in order to test the core excitation model.[1] In this model some levels in an odd nucleus arise from a weak coupling between an odd particle (or hole) and an excitation mode of the even-even core. This coupling will give rise to a multiplet of levels with spins $I' = \ell + j$, $\ell + j - 1$, ----, $\ell - j$, where ℓ is the spin of the excited level in the core nucleus and j is the spin of the odd nucleus in its ground state. In first approximation, the "center of gravity" of this multiplet will coincide with the corresponding level in the core-nucleus. The excitation of the multiplet and the decay to the ground state will be related to the level in the core nucleus.

Several experimental groups[2,3] have investigated this model by measuring angular distributions of inelastically scattered α-particles from even-even nuclei and their neighbors. Inelastic α-scattering has been found to favor the excitation of collective levels, and in cases where the adiabatic theory of inelastic scattering is valid, it is known[4] that the angular distributions of α-particles scattered from the multiplet are related to the angular distribution from the core level by the formula: $(d\sigma/d\Omega)(\ell; I = j \rightarrow I') = [(2I' + 1)/(2\ell + 1)\ (2I + 1)](d\sigma/d\Omega)(0 \rightarrow \ell)$ in odd nucleus = even-even core. Harvey, et al.,[3] found a doublet in N^{15} arising from a $p_{1/2}$ hole coupled to the 3^- collective excitation of the O^{16} core. On the other hand, Bruge, et al.,[2,3] found a multiplet of five (or six) levels in Cu^{63} and Cu^{65}, where only a quadruplet is expected.

The present study was undertaken because the doubly magic Pb^{208} nucleus can be expected to serve as a good core for the Pb^{207} and Bi^{209} nuclei. Angular distributions of inelastically scattered α-particles of 42 MeV incident energy were obtained for the levels in Pb^{207}, Pb^{208}, and Bi^{209} shown in Table 6-1. The scattered α-particles were detected in Li-drifted silicon detectors. The overall energy resolution was 90 to 110 keV. The most strongly excited level

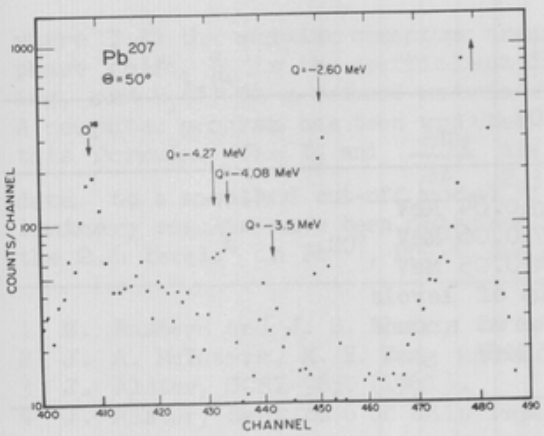

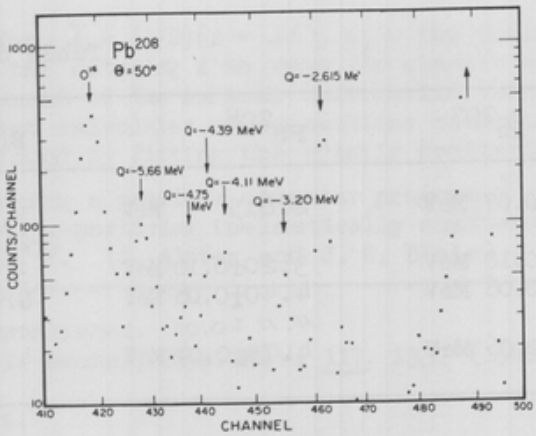

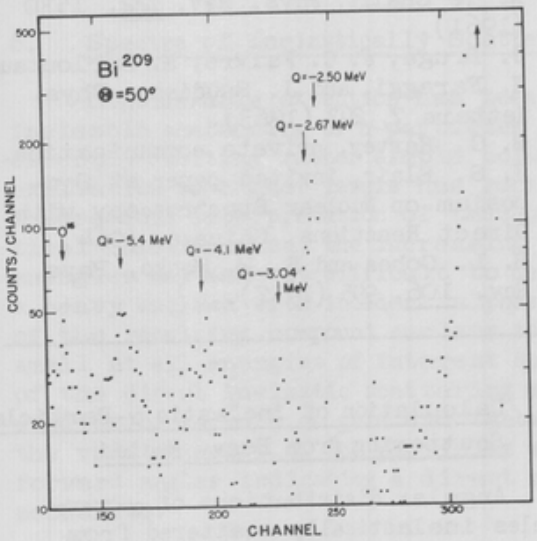

Fig. 6-1 Energy spectra for inelastically scattered α particles of 42 MeV incident energy taken at 50 degrees on a) Pb^{207}, b) Pb^{208}, c) Bi^{209}.

occurred at 2.6 MeV excitation in all three nuclei, as has been found previously with inelastic proton scattering.[5] The intensities of the other levels of Table 6-1 were from three to six times smaller than the 2.6 MeV levels. Figure 6-1 shows the spectra for Pb^{207}, Pb^{208} and Bi^{209} taken at 50 degrees. Figure 6-2 shows the angular distributions for the 2.60 level in Pb^{207}, the 2.615 level in Pb^{208}, and the sum of the 2.50 and 2.67 MeV levels in Bi^{209}. Within statistical errors these angular distributions are identical in shape as well as in magnitude. We therefore identify the 2.60 MeV level in Pb^{207} and the two groups in Bi^{209} as being the core excitation levels corresponding to the 3^- level in Pb^{208} at 2.615 MeV. In this picture one expects a doublet in in Pb^{207} and a multiplet of seven levels in Bi^{209}. Since no broadening beyond our resolution of 100 keV was observed in Pb^{207}, one has to conclude that the coupling is very weak. The levels in Bi^{209} combine into two groups, where the 2.67 MeV group has about one-fourth the intensity of the 2.50 MeV group. Both groups exhibit the same angular distributions shown in Figure 6-2, as well as those of the other levels of Table 6-1, do not show the usually pronounced diffraction structure because of the strong Coulomb field. (J. Alster, D. L. Hendrie, and R. J. Peterson)

Table 6-1

Pb^{207}	Pb^{208}	Bi^{209}
2.60±0.07 MeV	2.615 MeV	2.50±0.04 MeV 2.67±0.06 MeV
3.52±0.10 MeV	3.20±0.10 MeV	3.04±0.05 MeV
4.08±0.06 MeV	4.40±0.06 MeV 4.77±0.06	Group of levels centered around
4.27±0.06 MeV	4.75±0.04 MeV	4.15 MeV

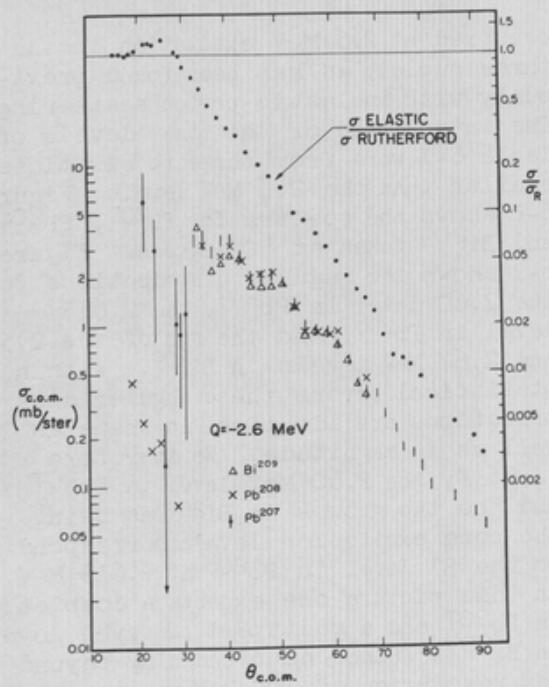

Fig. 6-2 Angular distributions of inelastically scattered 42 MeV α's from the 2.6 MeV levels in Pb^{207}(o), Pb^{208}(x) and Bi^{209}(Δ)

1 A. de Shalit, Phys. Rev. 122, 1530 (1961).
2 G. Bruge, J. C. Faivre, M. Barloutaud, H. Faraggi, and J. Saudinos, Phys. Letters 7, 203 (1963).
3 B. G. Harvey, private communication.
4 J. S. Blair, invited paper at Symposium on Nuclear Spectroscopy with Direct Reactions, Chicago, 1964.
5 B. L. Cohen and S. W. Mosko, Phys. Rev. 106, 995 (1957).

7. Calculation of Inelastic α-Particle Scattering from Heavy Nuclei

Angular distributions of α-particles inelastically scattered from heavy targets, such as lead, can be calculated using a model based on the adiabatic approximation which includes the Coulomb distortion.[1] This theory gives the formula:

$$f_{I,M_I;0,0} = \frac{-i}{2}(2I+1)\sum_{\ell,\ell'} i^{\ell-\ell'}(2\ell'+1)^{1/2}\, e^{i(\sigma_\ell+\sigma_{\ell'})} \langle \ell' I, -M_I, M_I \mid \ell 0\rangle$$

$$\langle \ell' I, 0\,0 \mid \ell\, 0\rangle \frac{\partial \eta}{\partial \ell}\bigg|_{\bar{\ell}} \sqrt{\quad}_{\ell'}^{-M_I}(\theta, 0)$$

$$\frac{d\sigma}{d\Omega}(0 \to I) = \sum_{M_I} \left| f_{I,M_I,0,0} \right|^2 C_1^2 \quad (I)$$

where I is the angular momentum transfer, $\bar{\ell} = (1/2)(\ell + \ell')$, σ_ℓ = the Coulomb phase shift, η_ℓ is the coefficient of the outgoing ℓ'th wave for elastic scattering, and $C_1(I)$ is a reduced matrix element of the nuclear deformation coordinate. A computer program has been written that calculates cross sections according to this formula. The $\eta_{\bar{\ell}}$ and $\frac{\partial \eta_{\bar{\ell}}}{\partial \ell}$ are found by fitting the elastic scattering data to a smoothed cut-off model[2,3] using a previous computer program.[3] Preliminary results have been obtained for α-particles inelastically scattered from the 2.6 levels[4] in Pb^{207}, Pb^{208} and Bi^{209}. (J. Alster and J. S. Blair)

---

1 N. Austern and J. S. Blair, to be published.
2 J. A. McIntyre, K. H. Wang and L. C. Becker, Phys. Rev. 117, 1337 (1960).
3 J. Alster, UCRL-9650 (1961).
4 J. Alster, Section 6 of this report.

---

8. Spectra of Inelastically Scattered Alpha Particles from Heavy Nuclei

Considerable attention has been directed in recent years to a study of the inelastic scattering of α-particles to low-lying nuclear levels as a way of directly exciting rather simple collective motions of nuclei.[1] Direct nuclear excitation to higher levels has received comparatively little attention. A theoretical interpretation of this could be much more complex, and, as a practical consideration, the increasing importance of evaporation at lower emission energies may make it difficult to determine the direct component. However, for a heavy nucleus with incident alphas in the region of 40 MeV, the temperature of the resulting compound nucleus is low. Consequently, evaporation will remain small at all energies of interest down to the Coulomb barrier, and a clean study of the direct inelastic scattering may be possible for heavy nuclei. Recent studies of (α, α') on gold and tantalum at 30 MeV,[2] 40 MeV,[3] and 48 MeV[4] do show the vast majority of the particles above the Coulomb barrier to be peaked toward forward angles indicating a direct rather than a compound nucleus reaction mechanism.

These investigations also revealed several unexpected features at 30 and 40 MeV that did not appear at 48 MeV bombarding energy. In particular, at 40 MeV there was little indication of the expected cut-off for alpha particle emission below the Coulomb barrier. Furthermore, the appearance of gross structure in both angle and excitation energy in the 30 and 40 MeV work suggests that serious consideration must be given to problems of background, particle identification and target contamination. The preliminary experiments reported here were designed to resolve these inconsistencies and provide a clearer picture of direct reactions producing high nuclear excitation.

42 MeV α-particles were used to bombard clean, self-supporting foils of tantalum (10.0 mg/cm^2) and gold (10.3 mg/cm^2). Signals from a dE/dx detector (either a thin gas proportional counter or a 50 micron transmission silicon detector) and a thicker stopping detector were combined to identify the doubly-charged reaction products. Figure 8-1 shows the energy spectra of the emitted α-particles from tantalum taken at 20° intervals between 40° and 140°. The data for gold are similar.

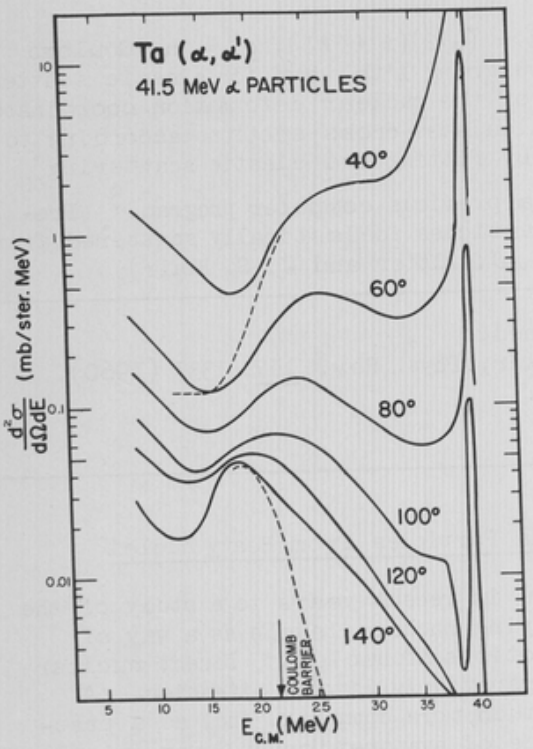

Fig. 8-1 Energy spectra of doubly-charged particles at various angles from tantalum bombarded with 41.5 MeV α-particles.

The forward dependence of the distributions at all energies, reported previously, is verified, and the drop in cross-section for energies below the Coulomb barrier is seen at all angles. For angles greater than 100° the yield near 18 MeV levels out, suggesting that the contribution of evaporated α-particles is beginning to dominate. An approximate calculation predicts an evaporative distribution peaking at 19 MeV, with a cross section close to that observed experimentally. The predicted rate of fall with increasing energy is considerably more than experiment, however (see dotted fit to 140° curve in Figure 8-1), indicating the importance of direct emission even at these backward angles.

The observed increase in yield below 12 MeV includes many effects, notably: beam degradation in the entrance collimator and detector aperture, scattering from light contaminants, especially carbon and oxygen, and nuclear reactions induced by α-particles in the detector material. Slit scattering in the beam collimating system is the most important of these, and the dotted branch of the 40° curve in Figure 8-1 shows the improvement obtained when the collimator was removed.

The above measurements show that most of the alphas are emitted with energies greater than 20 MeV, and it was decided to investigate this region in detail with improved resolution. A silicon detector was used to measure α-particles with energies up to 42 MeV with 150 keV resolution. Only those particles depositing more than 20 MeV were recorded. Singly-charged particles could not lose more than about 18 meV in the sensitive region of the detector and thus did not contribute to the energy region of interest.

Inelastic spectra were obtained for targets of natural Ta, Au, Pt, and Bi. The results for gold at four scattering angles are shown in Figure 8-2. The data at 40° and 60° agree with the earlier results obtained using the E - dE/dx particle identification system, while the 45° and 50° curves confirm the previously observed trend of a smooth, monotonic decrease with angle at all energies. Below 25° the inelastic contribution is masked by effects including low-energy α-particle contamination of the incident beam and the interaction of the intense flux of elastically scattered particles with the detector and its aperture. This background typically has a cross-section per MeV 1/500 th to 1/1000 th of the elastic cross section and represents an unimportant correction to the measurements at 40° and above.

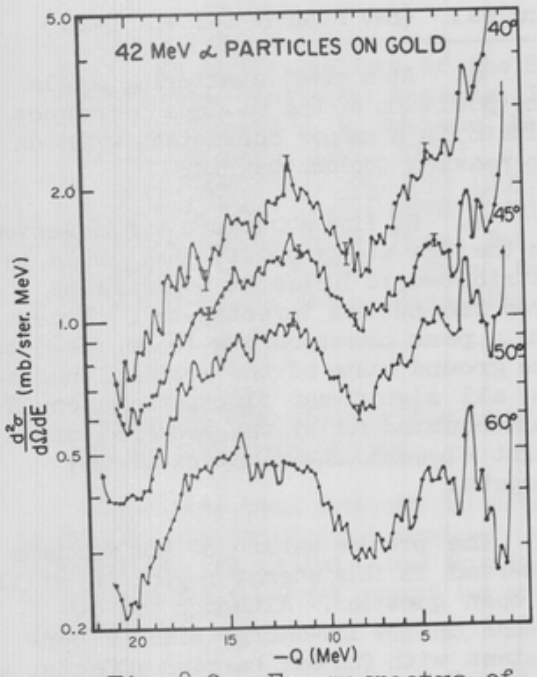

Fig. 8-2 Energy spectra of charged particles emitted at 40°, 45°, 50° and 60° from gold bombarded with 42 MeV α-particles.

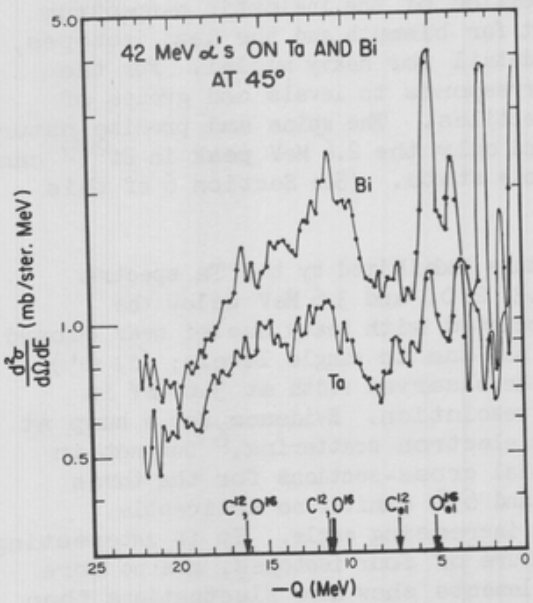

Fig. 8-3 Energy spectra of charged particles emitted at 45° from bismuth and tantalum bombarded with 42 MeV α-particles.

The outstanding feature of each of the spectra in Figure 8-2 is the grouping of the emitted particles into two distinct energy regions separated by a well-defined minimum. The region extending several MeV below the elastic peak includes the excitation of low-lying energy levels also observed in the inelastic scattering of other charged particles. The structure in this region corresponds to discrete groups of excited states. Proceeding from the minimum at about 7 MeV below the elastic peak, the cross section rises to form a broad maximum at an excitation between 12 and 15 MeV. As noted earlier, the fall-off below this region is consistent with the expected influence of the strong Coulomb barrier. The data for the other three nuclei studied show the same gross features as described above for Au. Forty-five degree spectra for Ta and Bi are given in Figure 8-3; the Pt data are almost identical with the Au data in Figure 8-2.

Since even the qualitative behavior of the low-energy maximum was previously unknown, the main emphasis of the present work has been to compile relevant experimental information about this interesting feature of inelastic scattering. Some of the properties are as follows:

a. At a given scattering angle the magnitude of the cross section increases with nuclear size (see Figure 8-3).

b. The minimum separating the two regions always occurs near 7 MeV excitation energy, independent of scattering angle and target nucleus, at least for the rather limited range of nuclei studied.

c. The position of the low-energy maximum appears to decrease slightly with increasing angle producing relatively more low-energy particles at higher

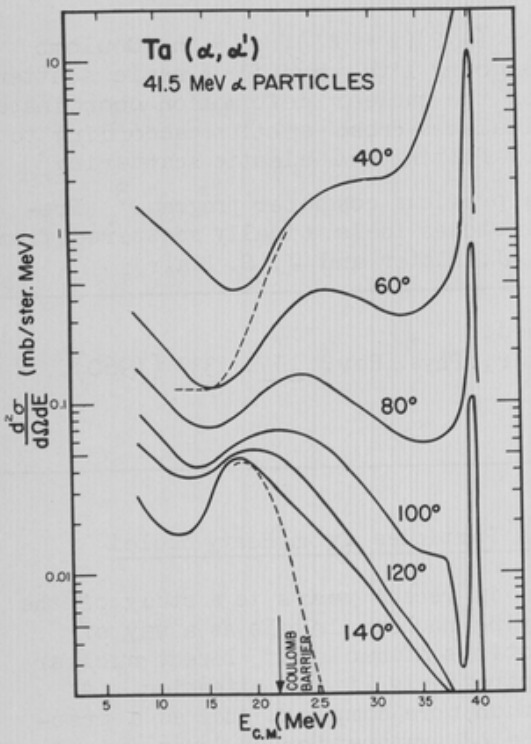

Fig. 8-1 Energy spectra of doubly-charged particles at various angles from tantalum bombarded with 41.5 MeV α-particles.

The forward dependence of the distributions at all energies, reported previously, is verified, and the drop in cross-section for energies below the Coulomb barrier is seen at all angles. For angles greater than 100° the yield near 18 MeV levels out, suggesting that the contribution of evaporated α-particles is beginning to dominate. An approximate calculation predicts an evaporative distribution peaking at 19 MeV, with a cross section close to that observed experimentally. The predicted rate of fall with increasing energy is considerably more than experiment, however (see dotted fit to 140° curve in Figure 8-1), indicating the importance of direct emission even at these backward angles.

The observed increase in yield below 12 MeV includes many effects, notably: beam degradation in the entrance collimator and detector aperture, scattering from light contaminants, especially carbon and oxygen, and nuclear reactions induced by α-particles in the detector material. Slit scattering in the beam collimating system is the most important of these, and the dotted branch of the 40° curve in Figure 8-1 shows the improvement obtained when the collimator was removed.

The above measurements show that most of the alphas are emitted with energies greater than 20 MeV, and it was decided to investigate this region in detail with improved resolution. A silicon detector was used to measure α-particles with energies up to 42 MeV with 150 keV resolution. Only those particles depositing more than 20 MeV were recorded. Singly-charged particles could not lose more than about 18 meV in the sensitive region of the detector and thus did not contribute to the energy region of interest.

Inelastic spectra were obtained for targets of natural Ta, Au, Pt, and Bi. The results for gold at four scattering angles are shown in Figure 8-2. The data at 40° and 60° agree with the earlier results obtained using the E - dE/dx particle identification system, while the 45° and 50° curves confirm the previously observed trend of a smooth, monotonic decrease with angle at all energies. Below 25° the inelastic contribution is masked by effects including low-energy α-particle contamination of the incident beam and the interaction of the intense flux of elastically scattered particles with the detector and its aperture. This background typically has a cross-section per MeV 1/500 th to 1/1000 th of the elastic cross section and represents an unimportant correction to the measurements at 40° and above.

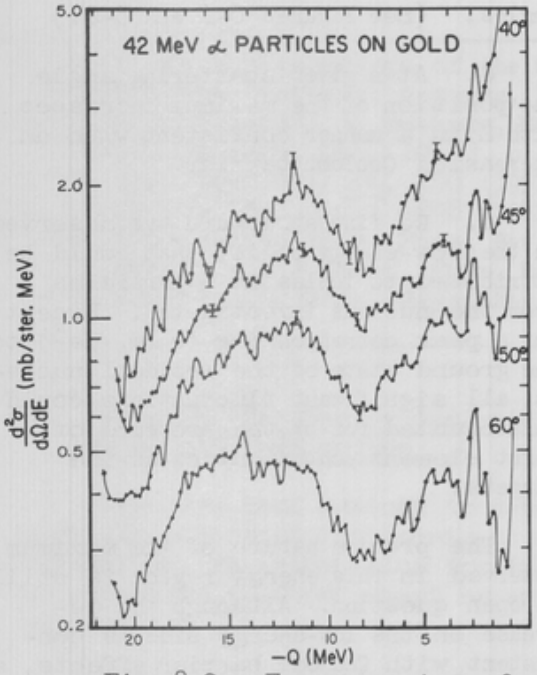

Fig. 8-2 Energy spectra of charged particles emitted at 40°, 45°, 50° and 60° from gold bombarded with 42 MeV α-particles.

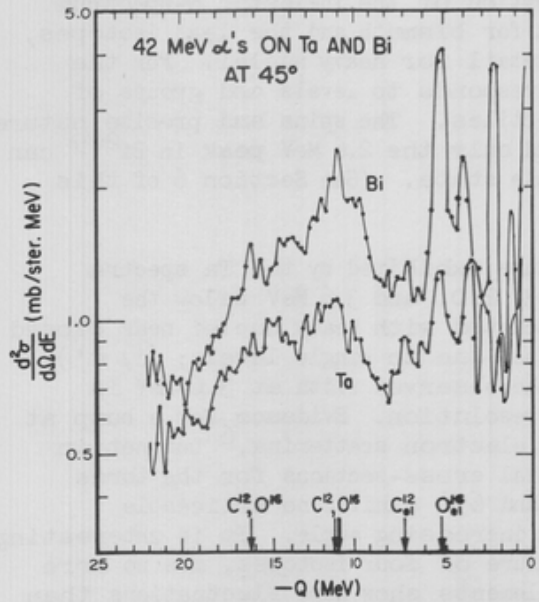

Fig. 8-3 Energy spectra of charged particles emitted at 45° from bismuth and tantalum bombarded with 42 MeV α-particles.

The outstanding feature of each of the spectra in Figure 8-2 is the grouping of the emitted particles into two distinct energy regions separated by a well-defined minimum. The region extending several MeV below the elastic peak includes the excitation of low-lying energy levels also observed in the inelastic scattering of other charged particles. The structure in this region corresponds to discrete groups of excited states. Proceeding from the minimum at about 7 MeV below the elastic peak, the cross section rises to form a broad maximum at an excitation between 12 and 15 MeV. As noted earlier, the fall-off below this region is consistent with the expected influence of the strong Coulomb barrier. The data for the other three nuclei studied show the same gross features as described above for Au. Forty-five degree spectra for Ta and Bi are given in Figure 8-3; the Pt data are almost identical with the Au data in Figure 8-2.

Since even the qualitative behavior of the low-energy maximum was previously unknown, the main emphasis of the present work has been to compile relevant experimental information about this interesting feature of inelastic scattering. Some of the properties are as follows:

a. At a given scattering angle the magnitude of the cross section increases with nuclear size (see Figure 8-3).

b. The minimum separating the two regions always occurs near 7 MeV excitation energy, independent of scattering angle and target nucleus, at least for the rather limited range of nuclei studied.

c. The position of the low-energy maximum appears to decrease slightly with increasing angle producing relatively more low-energy particles at higher

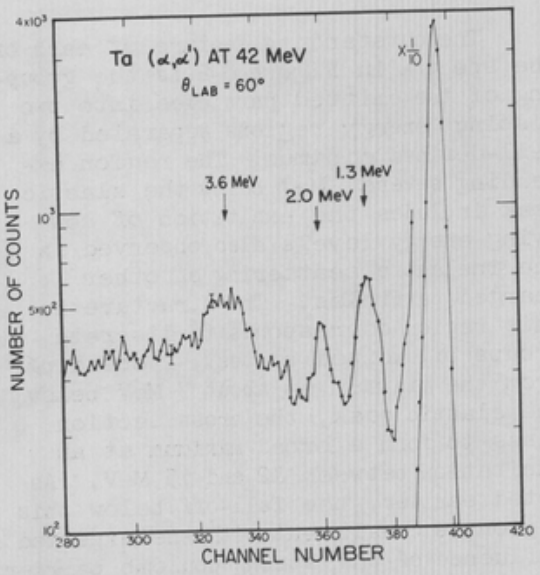

Fig. 8-4 Pulse height spectrum of scattered α-particles from tantalum at 60°.

angles. (See Figures 8-1 and 8-2.)

d. At a given scattering angle the position of the maximum increases with Z in a manner consistent with an increasing Coulomb barrier.

e. No fine structure was observed in the low-energy region that could be attributed to inelastic α-particles from the nucleus investigated. Except for a peak corresponding to (α, He^3) to the ground state of the residual nucleus, all significant fluctuations could be accounted for by the presence of light element contamination in the targets.

The precise nature of the maximum observed in this energy region is still an open question. Although the decrease on the low-energy side is consistent with Coulomb barrier effects, a broad nuclear resonance may be involved as well. Studies of this region of excitation with higher bombarding energies should help to resolve this question.

Certain features of the high-energy portion of the inelastic α-spectrum also appear to merit further study. Except for bismuth and the lead isotopes, these have not been investigated in great detail for heavy nuclei. For the most part, the structure in this region corresponds to levels and groups of levels previously observed with other projectiles. The spins and precise nature of these excitations are largely unknown and only the 2.6 MeV peak in Bi^{209} can safely be attributed to a collective octupole state. (See Section 6 of this report.)

Particularly interesting is the structure exhibited by the Ta spectra (Figure 8-4). The well-defined peaks at 1.3, 2.0, and 3.6 MeV below the elastic peak contain strength normally associated with heavy nuclei near closed shells. The 1.3 MeV and 3.6 MeV peaks are not due to single levels; (d, d') results[5] show a splitting at 1.3 MeV, and the observed width at 3.6 MeV is much greater than the present experimental resolution. Evidence for a bump at 3.6 MeV has also been observed in inelastic electron scattering,[6] but not in (p, p')[7] or (d,d')[5] experiments. Differential cross-sections for the three groups taken at 2.5° intervals between 40° and 65° exhibit no noticeable oscillation and decrease monotonically with increasing angle. It is interesting to note that the spectra of platinum, a mixture of four isotopes, are no more complex than those of gold, although both elements show more fluctuations than tantalum. Moreover, there is a hint of a close correspondence in the structure between gold and platinum in the 1 to 3 MeV region of excitation. (I. Halpern, J. Lilley, and N. Stein)

1 J. S. Blair, Proceedings of the Symposium on Nuclear Spectroscopy with Direct Reactions, Argonne, Illinois, 1964.
2 C. R. Gruhn and L. W. Swenson, Massachusetts Institute of Technology Progress Report, (May, 1963), p. 106.
3 G. Igo, Phys. Rev. 106, 256 (1957).
4 G. Merkel, UCRL Report 9898 (1961).
5 B. Cohen and R. Price, Phys. Rev. 123, 283 (1961).
6 H. Kendall and J. Oeser, Phys. Rev. 130, 245 (1963).
7 B. Cohen and A. Rubin, Phys. Rev. 111, 1568 (1958).

9. Magnetic Spectrometer Analysis of Alpha Particle Scattering: Q Value Determinations

Data have been obtained to determine accurate Q values from inelastic alpha particle scattering experiments on a number of nuclei. Q values and relative intensities are listed below for Fe^{56}, Ni^{60}, Ni^{62} and Zr^{90}. All uncertainties in energy are ± 10 keV except as noted. Data were taken at a laboratory scattering angle of 20°.

Data also were obtained for Si^{28}, Cr^{52}, and Ge^{72} and are now being analyzed. (D. L. Hendrie and R. J. Peterson)

-Q (MeV)		Intensity (Arbitrary Units)
	Fe^{56}	
0.845		200
2.095		30
2.660		140
3.18	+50,-10keV	85
3.393		40
3.611		35
3.844		45
4.538		150
4.725		40
4.894		35
5.182		80
5.285		85
5.746		35
5.924		35
6.28	±20keV	35
6.477		30
6.787		30
7.082		45
	Ni^{62}	
1.172		270
2.312		55
3.23	+50,-10keV	60
3.531		20
3.774		160
4.154		70
4.670		25
4.790		25
5.035		40
5.324		60
5.686		70
5.718		40
6.078		40
6.191		40
6.577		35
7.064		25

-Q (MeV)		Intensity (Arbitrary Units)
	Ni^{60}	
1.332		300
2.163		40
2.501		130
3.15	+50,-10keV	210
3.342		85
3.713		70
4.067		280
4.348		55
4.530		60
5.103		230
5.429		55
5.943		80
6.255		85
	Zr^{90}	
2.183		300
2.327		100
2.745		180
3.066		40
3.296		60
3.466		30
3.873		90
4.344		60
5.145		40
5.376		55
5.759		85
6.649		65
7.941		80

III. ANGULAR CORRELATIONS BETWEEN PHOTONS AND SCATTERED PARTICLES

10. Alpha-Gamma Correlations on Mg^{24}

For inelastic alpha scattering exciting a 2^+ level which then decays to the 0^+ ground state, the most general alpha-gamma correlation pattern in the scattering plane can be shown to be of the form $A + B \sin^2 2(\theta_\gamma - \theta_0)$. θ_0 is the gamma emission angle, and A, B, and θ_0 are parameters determined by the nuclear reaction mechanisms. Adiabatic calculations,[1] which have provided good agreement with inelastic differential cross sections, predict that A is zero and that θ_0 lies along the adiabatic recoil axis. Previous results[2] on the 2^+ level in C^{12} at 4.43 MeV have shown large deviations from this theory. A similar experiment was started on the 1.37 MeV level of Mg^{24} to see if closer agreement would be found where adiabatic conditions are better fulfilled.

Preliminary results on the behavior of θ_0 are shown in Figure 10-1. Also shown in the figure are the results of computer calculations which have recently become available. Distorted wave Born approximation calculations[3] yield results which are at least in qualitative accord with the observed data. The more sophisticated coupled-channel calculations[3,4] unexpectedly seem to fit the data less well.

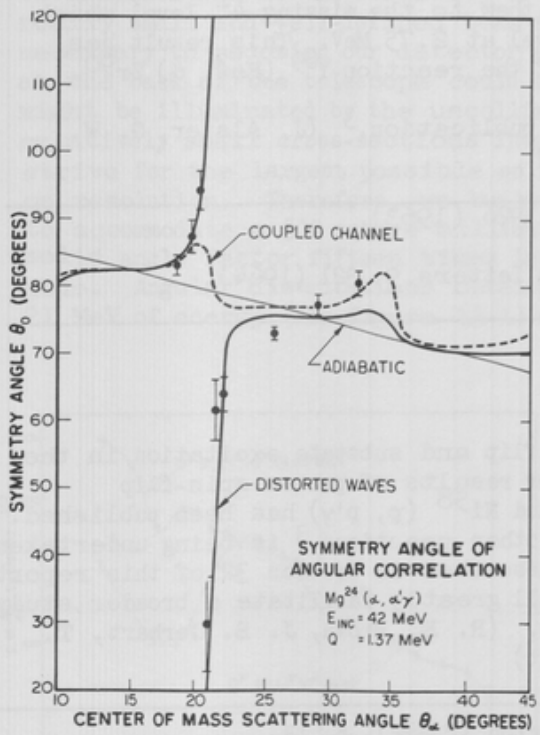

Fig. 10-1 Plot of θ_0 versus laboratory scattering angle. Theoretical predictions are from References 10-1, 10-3, and 10-4.

Data taking capability has been improved by use of a larger area solid state α-detector and by a new fast coincidence system. The use of a time-to-pulse height system for evaluation of accidental coincidences has not proven feasible (see Section 27 of this report). Present plans are to increase the range of the data to larger alpha angles. Calculations are also being performed to see if better fits can be obtained by varying parameters in the DWBA and coupled-channel theories. (J. Alster, G. W. Farwell, D. L. Hendrie, and R. J. Peterson)

1 J. S. Blair and L. Wilets, Phys. Rev. 121, 1493 (1961).
2 D. K. McDaniel, D. L. Hendrie, R. H. Bassel and G. R. Satchler, Phys. Letters 1, 295 (1962).
3 G. R. Satchler, Private Communication.
4 J. G. Wills, Ph.D. Thesis, University of Washington (1963).

11. Location of the "Missing" 4^- Level in Zr^{90}

Shell model calculations have successfully described many of the low-lying levels of Zr^{90}. Experiments have identified all of the expected levels with exception of the 4^- state predicted to lie around 3 MeV. Recent neutron inelastic scattering work[1] has revealed a threshold at 2.75 MeV for excitation of a state that undergoes gamma decay (430 keV) to the 5^- state at 2.32 MeV with appreciable probability (about 30%). However, the known 3^- collective level at this energy would be expected to decay almost entirely to the 2^+ state at 2.18 MeV, and it was suggested[1] that the "missing" 4^- level is excited in neutron inelastic scattering.

Our experiment made use of the preferential excitation of the 3^- collective level through alpha particle inelastic scattering. (Excitation of the 4^- state in alpha scattering would be strongly inhibited both because of the "unnatural parity" of this state and because of its single particle nature.) In observation of the de-excitation gamma rays in coincidence with the appropriate inelastic alpha group, we find a negligibly small 430-keV gamma component representing the transition to the 5^- level. (The relative transition probability for 430 keV versus 570 keV is 1.7±2.7%.) Following the suggestion of Wagner et. al., we attribute the 430-keV gamma ray seen by them to the missing 4^- level which forms an unresolved doublet with the 3^- level at 2.75 MeV. This result has been confirmed[2] recently through studies of the reaction Y^{89} (He^3, d) Zr^{90}.

Further details are given in a recent publication.[3] (J. Alster, G. W. Farwell, D. L. Hendrie, and R. J. Peterson)

---

1 Wagner, Shunk, and Day, Phys. Rev. 130, 1926 (1963).
2 R. B. Day, private communication.
3 D. L. Hendrie and G. W. Farwell, Physics Letters 9, 321 (1964).

---

12. Proton-Gamma Ray Angular Correlations

The previously reported work[1] on spin flip and substate excitation in the reaction C^{12} (p, p'γ), together with further results of proton spin-flip measurement in the reactions Mg^{24} (p, p'γ) and Ni^{58} (p, p'γ) has been published.[2] Further investigation of these, as well as other reactions,[3] is being undertaken with an improved particle detector system described in Section 32 of this report. The new tandem Van de Graaff accelerator will greatly facilitate a broader study of the energy dependence of these reactions. (R. E. Brown, J. B. Gerhart, T. Hayward, W. A. Kolasinski, and F. H. Schmidt)

---

1 Cyclotron Research, University of Washington (1962), p. 13.
2 F. H. Schmidt, R. E. Brown, J. B. Gerhart, and W. A. Kolasinski, Nucl. Phys. 52, 353 (1964).
3 Cyclotron Research, University of Washington (1963), p. 14.

IV. PICKUP AND OTHER INTERACTIONS

13. Alpha Particle Pickup Reactions

We have continued our investigation of (d, Li^6) reactions in an attempt to study alpha-particle clustering on the surface of light and intermediate weight nuclei as was described in last year's report.[1] Particles are detected with a gas-filled proportional dE/dx counter and solid state E counter telescope package. Particle identification and separation are accomplished with a pulse stretcher and x - y oscilloscope system which has been described earlier.[2] Energy spectra and angular distributions have been taken on targets of zinc and magnesium, although these were complicated by pile-up difficulties in our electronics. We found that we could avoid these problems by running without a beam collimator as this greatly reduced the background in our scattering chamber. As a consequence of this we have to align the external beam system of the cyclotron with the aid of a television camera and phosphorescent target. We are fortunate to have well-regulated focus and analyzing magnets in the external beam system so that there is no problem of the beam spot wandering around on the target. Moreover, the new split-faraday-cup-beam current measuring system[3] gives us a very sensitive indication of the stability of our beam. Since it is difficult to obtain a really small and well-defined beam spot without a beam collimator, we found it necessary to redesign our detector package to make certain that the E detector at the back of the telescope could be seen by every point on the target which might be illuminated by the uncollimated beam. In addition to this, the relatively small cross-sections involved in these reactions make it desirable to strive for the largest possible solid angle compatible with one's requirements on resolution. Therefore, we built a new gas proportional counter large enough to accommodate a 300 square millimeter surface barrier E detector giving us a solid angle factor fifteen times larger than that which was previously obtainable. Angular distributions obtained on O^{16} targets with incident deuterons of 21 MeV of energy (see Figure 13-1) were found to be essentially unaffected by variations of up to roughly 400 keV in the incident deuteron energy. This lack of any strong energy dependence is highly suggestive of a direct reaction mechanism. Typical differential cross sections are a few hundred micro-barns/steradian. It is hoped that we can fit these data with suitable distorted wave calculations (J. B. Gerhart, P. Mizera, and F. W. Slee)

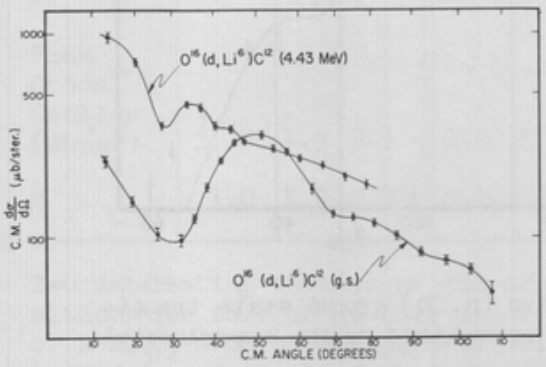

Fig. 13-1 (d, Li^6) reactions on O^{16} at 21 MeV incident energy.

1 Cyclotron Research, University of Washington (1963), p. 27.
2 Cyclotron Research, University of Washington (1962), p. 39.
3 Cyclotron Research, University of Washington (1964), p. 58.

14. DWBA Analysis of 40 MeV (p, d) Data

A distorted-wave analysis of 40 MeV (p, d) data on the $1f_{7/2}$ isotones (Ca^{48}, Ti^{50}, V^{51}, Cr^{52}, and Fe^{54}) has been carried out, employing the Oak Ridge Code "TSALLY."[1] The experimental data were obtained using the University of Minnesota Linear Proton Accelerator. DWBA calculations were made on the Pacific Northwest Computer Laboratory's IBM 709 facility.

The nuclei listed above form an especially interesting sequence in that all have "filled" $1f_{7/2}$ shells of 8 neutrons and differ only in the number of $1f_{7/2}$ protons. A model which is often proposed for these nuclei consists of an inert Ca^{40} core surrounded by a closed $1f_{7/2}$ shell of neutrons and (Z-20) $1f_{7/2}$ protons. An analysis of (p, d) reactions on such nuclei can be expected to yield information on the "purity of $(1f_{7/2})^n$ configuration, and to give some insight into the effect on the neutron configuration of adding protons as one progresses from Ca^{48} (with a "closed" $1d_{3/2}$ proton shell) to Fe^{54} (6 protons in the $1f_{7/2}$ shell).

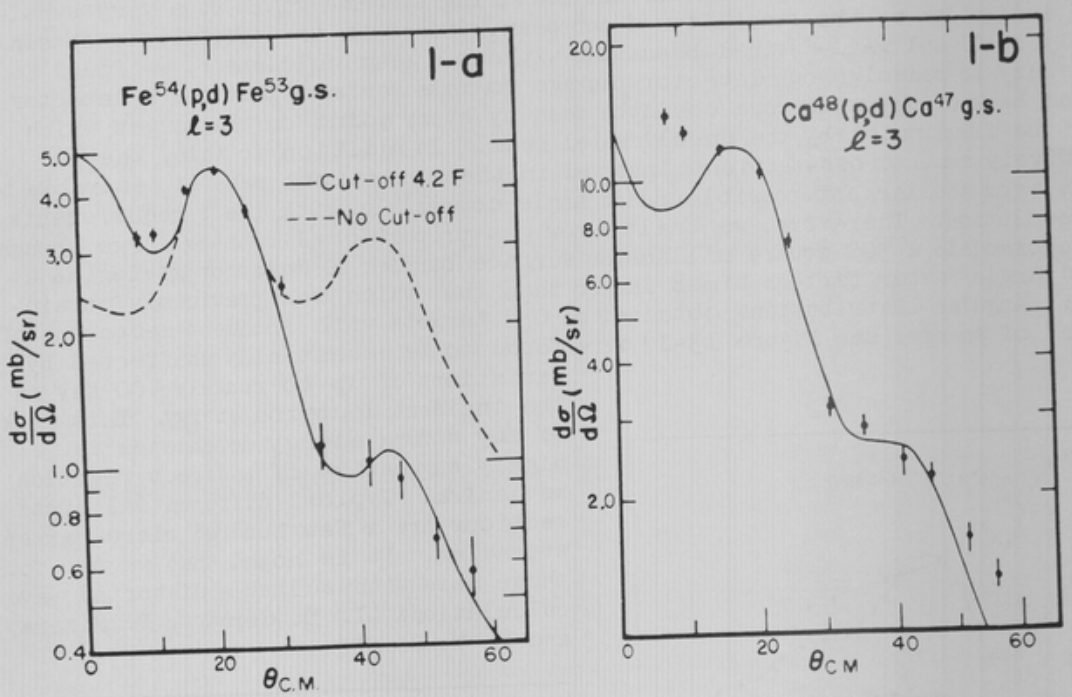

Fig. 14-1 Angular distributions for two (p, d) ground state transitions. The curves are DWBA calculations normalized to the experimental maxima.

Since proton and deuteron optical model parameters for the energies involved here (protons: 40 MeV, deuterons ≈ 30 MeV) were not generally available, it was necessary to make estimates based on data for lower energies. For the protons, the data of Fricke[2] for 40 MeV elastic scattering on Fe^{54} was used for all five nuclei studied in the analysis.[3] For the deuterons, an extrapolation was made from the data of Perey and Perey[4] using the "average geometry" ($r_0 = r_c = 1.15$, $a = 0.87$, $r_0 = 1.37$, $a' = 0.70$) and the "set A" parameters. Due to the large execution time of TSALLY (approximately three minutes for 15 partial waves in each channel), no attempt was made to further vary the parameters to improve individual fits. However, in all cases studied, it was found that a lower cut-off on the radial integration was necessary to obtain even qualitative agreement with the experimental data. A value of 4.2 F was chosen and used for all reactions studied. Figures 14-1a and 14-1b illustrate typical fits obtained with parameters selected as described above. The effect of the cut-off is shown for the reaction Fe^{54} (p, d) Fe^{53} (g.s.).

Spectroscopic factors for some of the strong transitions observed in the (p, d) experiment are listed together with other relevant data in Table 14-1.

Table 14-1

Experimental results for (p, d) reactions to the indicated residual nuclei. Spectroscopic factors arbitrarily normalized to those for Ca^{48} (p,d) Ca^{47}.

Residual Nucleus	Ca^{47}		Ti^{49}		V^{50}			Cr^{51}		Fe^{53}		
Excitation (MeV)	0	2.7	0	1.50	0	0.87	1.87	0	3.04	0	3.25	4.63
ℓ	3	1	3	1	3	3	1	3	1	3	1	3
Peak Cross Section (mb/sr)	11.8	4.9	9.3	0.5	3.5	3.2	2.6	6.5	4.0	4.5	2.0	1.6
S	1.0	1.0	0.86	0.1	0.33	0.30	0.62	0.61	1.2	0.44	1.3	0.19

Two interesting features of the data are: 1) the existence of strong $\ell = 1$ transitions for four of the five nuclei studied, suggesting appreciable admixtures of a $2p_{3/2}$ neutron configuration in the "closed" $1f_{7/2}$ shell; 2) a gradual dimunition of the $\ell = 3$ strength for the g.s. to g.s. transitions (g.s. to g.s. plus 0.87 MeV for V^{51}) as the proton number increases. This suggests that one effect of adding $1f_{7/2}$ protons to a nucleus with a closed $1f_{7/2}$ neutron shell is to "dilute" the neutron configuration in the ground state.

A summary of the results of this analysis has been submitted to the International Conference on Nuclear Physics (Paris). (C. D. Kavaloski)

---

1 R. H. Bassel, R. M. Drisko, and G. R. Satchler, ORNL-3240 (unpublished).
2 M. P. Fricke, University of Minnesota Thesis (unpublished).
3 Proton parameters used were: V = 44.8 MeV, W = 8.1 MeV, r_0 = 1.17F, r_c = 1.20F, a = 0.75F, r_0' = 1.40F, a' = 0.44F, W' = 0.
4 C. M. Perey and F. G. Perey, Phys. Rev. 132, 755 (1963).

---

15. The O^{16} (α, Be^8)C^{12} Reaction

In the course of measurements[1] on the Mg^{24} (α, Be^8)Ne^{20} reaction it was decided to investigate the O^{16} (α, Be^8) reaction in order to be able to correct the Mg^{24} data for known oxygen contamination of the target. It was found that the Mg^{24} results[1] were not altered substantially, and that the O^{16} (α, Be^8) reaction was itself of interest. We have therefore postponed further Mg^{24} work and have been investigating the O^{16} (α, Be^8)C^{12} reaction leading to the ground state and to the 4.43 MeV first excited state in C^{12}. Targets of NiO were employed; no appreciable Be^8 yield was observed for Ni.

Several changes have been made in the detector geometry previously reported.[1] At present three rectangular (5mm x 15mm) surface barrier detectors are mounted approximately 5° apart in the scattering chamber. The rectangular geometry allows us to increase the effective solid angle for Be^8 detection by about a factor of six over that obtained with the previous circular detectors while maintaining the same kinematic energy spread in the detectors. Three double coincidences are formed, one for each possible detector pair. The two outside detectors (10° apart) normally have a separation greater than the cone angle for Be^8 breakup and therefore detect "background" rather than Be^8 events. The other two coincidence requirements serve to detect Be^8 at two different laboratory angles. For every coincidence formed the pulses in each detector of the appropriate pair are added together. The sum spectra thus formed for each pair are routed to three separate quadrants of a 512-channel pulse height analyzer. Thus two angles and a "background" run are taken simultaneously.

To date angular distributions (mainly in the foreward hemisphere) have been measured for two bombarding energies 1.1 MeV apart (41.9 and 40.8 MeV). The results of these measurements are shown in Figure 15-1. The absolute cross section scale in the figure is based on a calculation of the effective solid angle for Be^8 detection carried out on an IBM 709 computer. The ground state cross section shows an appreciable dependence on incident energy. There is an increase in yield by about a factor of four and a shift of the oscillatory pattern when the energy is lowered from 41.9 to 40.8 MeV. In contrast to this the yield to the 4.43 MeV state is the same at the two energies, and the shape of the two distributions is similar though not identical.

It had been originally hoped that (α, Be^8) reactions could be interpreted as simple direct pickup processes. The large energy variation observed for the

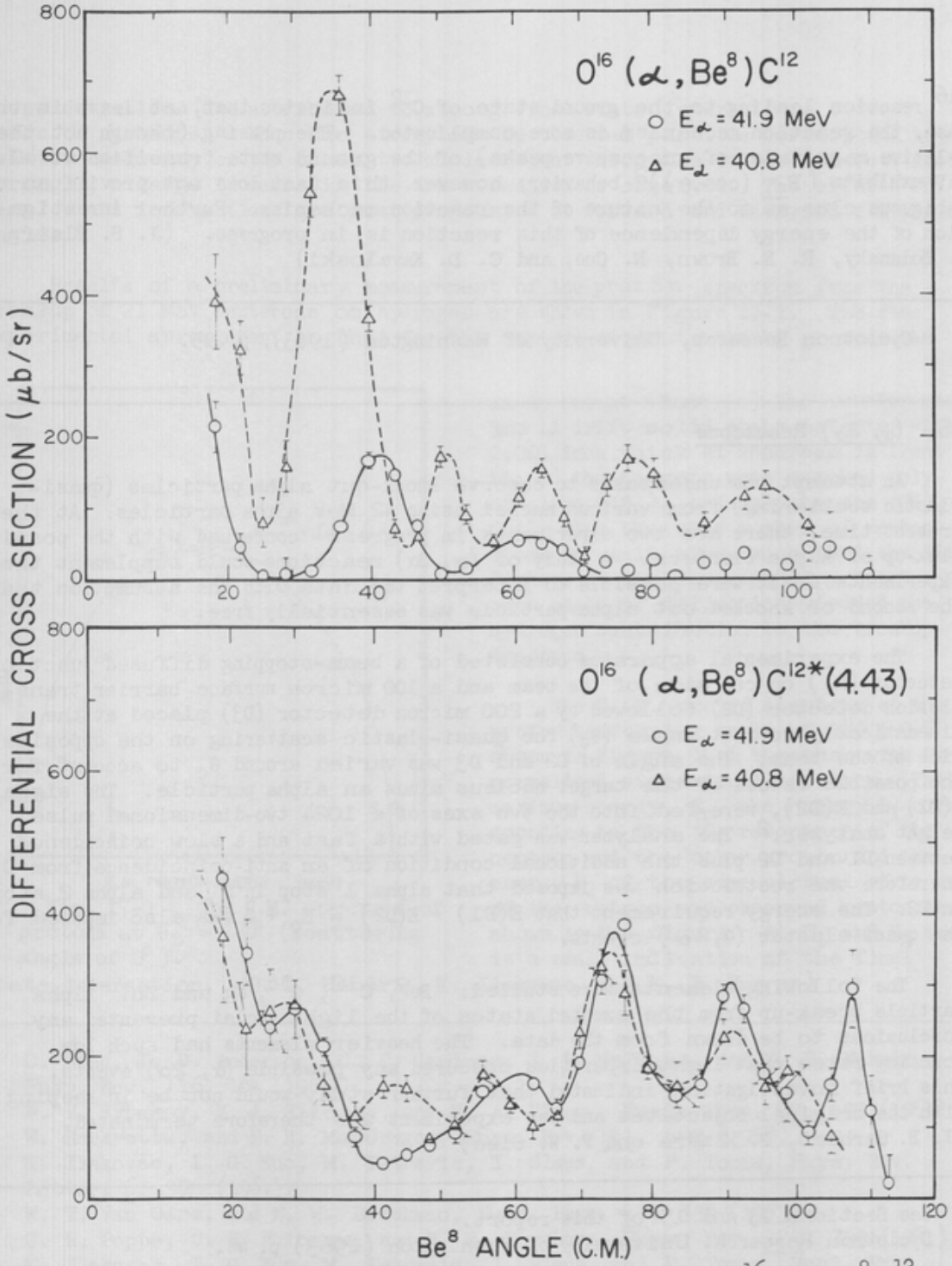

Fig. 15-1 Center-of-mass cross section for the reaction O^{16} (α, Be^8)C^{12} leading to the ground state (top figure) and to the first excited state (bottom figure) of C^{12} at bombarding energies of 41.9 and 40.8 MeV. The curves are drawn through the experimental points and have no other significance. (Erratum: Due mainly to a mistake in the original solid angle determination, the best present experimental cross sections are about 35% lower than indicated in the figure.)

O^{16} reaction leading to the ground state of C^{12} indicates that, at least in this case, the reaction mechanism is more complicated. The phasing (though not the relative magnitudes of successive peaks) of the ground state transition at 40.8 MeV exhibits $(P_{11}(\cos\theta))^2$ behavior; however, this fact does not provide an unambiguous clue as to the nature of the reaction mechanism. Further investigation of the energy dependence of this reaction is in progress. (J. S. Blair, D. Bodansky, R. E. Brown, N. Cue, and C. D. Kavaloski)

---

1 Cyclotron Research, University of Washington (1963), p. 25.

---

16. $(\alpha, 2\alpha)$ Reactions

An attempt was undertaken to observe knock-out alpha particles (quasi-elastic scattering) from various nuclei using 42 MeV alpha particles. At the present time, there are two experiments in progress[1] concerned with the possible pick-up of alpha clusters. A study of $(\alpha, 2\alpha)$ reactions would supplement these experiments if it were possible to interpret the data with the assumption that the second or knocked out alpha particle was essentially free.

The experimental apparatus consisted of a beam-stopping diffused junction detector (D1) on one side of the beam and a 100 micron surface barrier transmission detector (D2) followed by a 200 micron detector (D3) placed at the kinematically correct angle (θ_c) for quasi-elastic scattering on the opposite side of the beam. The angle of D2 and D3 was varied around θ_c to account for the possible recoil of the target nucleus minus an alpha particle. The signals, E(D1) and E(D2), were fed into the two axes of a 1024 two-dimensional pulse height analyzer.[2] The analyzer was gated with a fast and a slow coincidence between D1 and D2 plus the additional condition of an anti-coincidence from D3. Therefore the restriction was imposed that alpha 1 stop in D1 and alpha 2 stop in D2. The energy requirement that $E(D1) + E(D2) = E_o + Q$ was also imposed for the quasi-elastic $(\alpha, 2\alpha)$ events.

The following elements were studied: Be^9, C^{12}, O^{16}, Mg and Zn. Alpha particle break-up from the excited states of the light nuclei prevented any conclusions to be drawn from the data. The heavier elements had such low counting rates that light impurities obscured any possible $(\alpha, 2\alpha)$ events. This brief investigation indicated that further study would not be in keeping with the original objectives and the experiment was therefore terminated. (J. B. Gerhart, P. Mizera and F. W. Slee)

---

1 See Sections 13 and 15 of this report.
2 Cyclotron Research, University of Washington (1963) p. 44.

---

17. Breakup of Deuterons by Protons at 7 MeV C. M. Energy

Breakup of deuterons by nucleons over a wide range of energies has been extensively studied.[1,2] Measured continuum spectra of nucleons emerging from this reaction have shown strong deviations from the statistical distribution.

These deviations are attributed to strong final state interactions between pairs of nucleons.[3] When the energy of the observed particle corresponds to a relative velocity of the other two nucleons, at which the latter interact most strongly, a large increase in the cross section is observed. The effects of final state interactions are most pronounced at forward and backward scattering angles.[2]

Results of a preliminary measurement of the proton spectrum from the breakup of 21 MeV deuterons on hydrogen are shown in Figure 17-1. The same experimental arrangement as that for the capture of deuterons by protons was used, except that: a) the counter was a 3mm Li drift solid state detector with a 0.001 inch thick Ni absorber in front of it; b) the targets were matched polyethylene $(CH_2)_n$ and polystyrene $(CH)_n$ foils with the same number of carbon atoms per unit area, such that the difference of the corresponding spectra at each angle of deflection yielded the hydrogen contribution to the breakup spectrum.

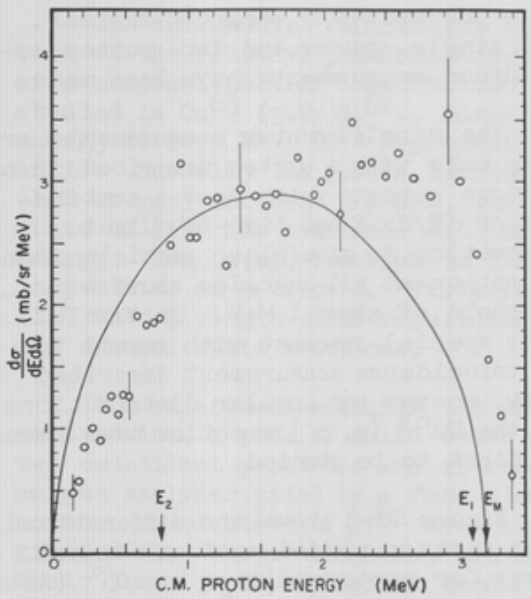

Fig. 17-1 The C.M. spectrum of protons at $\theta_p = 180°$ (scattering angle of 0°).

The C. M. proton spectrum at the proton scattering angle of $180 \pm 0.5°$ is shown in Figure 17-1 together with the normalized statistical spectrum. The maximum energy, E_m, the energy E_1 corresponding to the $^1S_0$ resonance of the neutron and the other proton, and the energy E_2 of the same virtual state but of the neutron and observed proton are shown in the figure. At E_1 and E_2 there is a small indication of the final state interaction. (D. L. Hendrie, K. Ilakovac, and E. B. Warren)

---

1 C. Wong, J. D. Anderson, C. C. Gardner, J. W. McClure, and M. P. Nakada, Phys. Rev. 116, 164 (1959).
B. V. Rybakov, V. A. Sidorov, and N. A. Vlasov, Nucl. Phys. 23, 491 (1961).
W. Heckrotte, and M. H. MacGregor, Phys. Rev. 111, 593 (1958).
K. Ilakovac, L. G. Kuo, M. Petravic, I. Slaus, and P. Tomas, Phys. Rev. Letters 6, 356 (1961).
W. T. Van Oers, and K. W. Brockman, Nucl. Phys. 47, 338 (1963).

2 C. H. Poppe, C. H. Holbrow, and R. R. Borchers, Phys. Rev. 129, 733 (1963).
K. Ilakovac, L. G. Kuo, M. Petravic, I. Slaus, and P. Tomas, Nucl. Phys. 43, 254 (1963).

3 R. M. Frank, and J. L. Gammel, Phys. Rev. 93, 463 (1954).
V. V. Komarov, and A. M. Popova, Nucl. Phys. 18, 296 (1960).

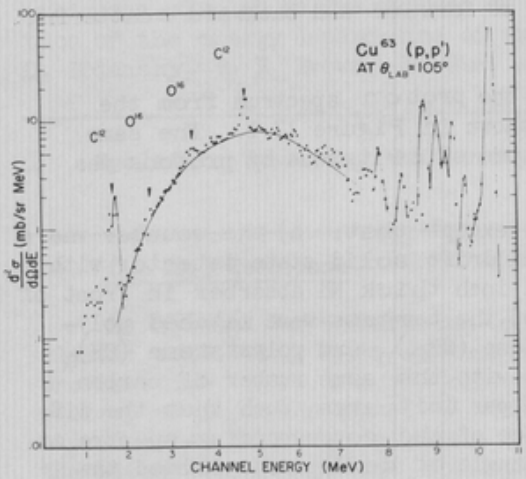

Fig. 18-1 Differential cross section versus channel energy for protons emitted at 105° lab angle in the proton bombardment of Cu^{63}.

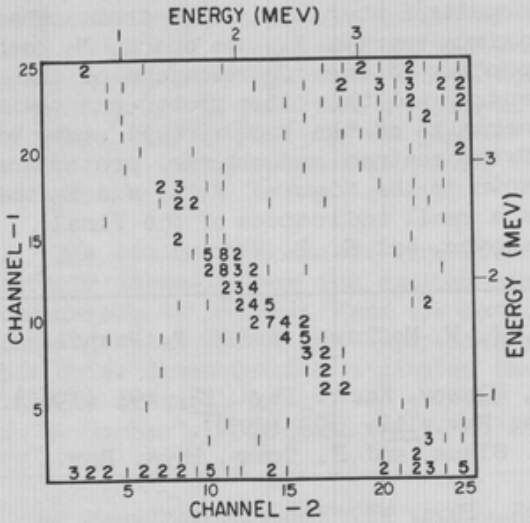

Fig. 18-2 Two-dimensional pulse height distribution for coincident charged particles emitted in the proton bombardment of Cu^{63}. The counters are at 90° to the beam direction.

18. Study of Low-Energy Proton Evaporation

The study of barrier penetration by low energy protons is continuing. The experiments concentrate on the measurement of the energy spectra of protons emitted with energy below the Coulomb barrier in reactions which are expected to be predominantly compound-nuclear. Both single-counter and two-counter coincidence measurements have been made.

The single-counter measurements are being made with a system described in a previous report[1] which uses a combination of dE/dx-E and time-of-flight information to give clear particle identification at all energies above a threshold of about 1 MeV. Because of their special interest with regard to the coincidence measurement described below, energy and angular distributions for the Cu^{63} (p, p') reaction have been the first to be studied.

Figure 18-1 shows the differential cross section plotted against channel energy for protons emitted at 105° (lab) in the bombardment of Cu^{63} by 10.5 MeV protons. The data shown is corrected for energy degradation of the protons in the target, but as yet includes no correction for background contributions from neutrons or gamma rays. This background amounts to about 10% of the observed spectrum at 2 MeV and is very much less at higher energy. Another type of background, conspicuous in the plotted spectrum, comes from target surface contamination. Qualitative features of the spectra and angular distribution are consistent with a predominantly compound-nuclear contribution to the reaction cross section at low emission energies, and increasing direct reaction contributions at higher emission energies. The low energy portion of the spectra are roughly isotropic; the present differen-

tial cross-section data shows isotropy within about 20% at 3 MeV from 50° to 130°. The more structured high energy region is forward-peaked.

According to the statistical theory, the shape of the energy spectrum below the Coulomb barrier is dominated by the energy dependence of the cross-section of the reaction inverse to the compound-nuclear decay being considered. At energies below the barrier, the energy dependence of the inverse cross-section is not very sensitive to the model chosen; a few preliminary calculations are in fair quantitative agreement with the observed spectrum shape and absolute cross-section.

The two-counter coincidence experiment is directed towards the determination of the relative probabilities of gamma ray and proton emission at the end of a compound-nuclear deexcitation cascade. The specific reaction being studied is Cu^{63} (p,2p)Ni^{62}. Since the incident proton beam is limited in energy to 10.5 MeV, Cu^{63} represents the most favorable choice of target because of its unusually low proton binding energy (6.11 MeV). Assuming 10.45 MeV (lab energy) incident protons, the (p,2p) reaction proceeding to the ground state of Ni^{62} has available 4.17 MeV (center of mass) for total proton kinetic energy. The (p,np) reaction is energetically impossible, eliminating neutron competition as a concern. Furthermore, the lowest excited state of Ni^{62} is at 1.17 MeV, giving a clean separation in total energy between the ground state and excited state reactions.

The experiment measures the energies of coincident charged particles emitted into a pair of solid-state detector telescopes. The energies of the two coincident particles are recorded in a 32 x 32 channel 2-dimensional pulse height analyzer gated by a fast-slow coincidence system. Since events leading to the ground state of Ni^{62} are characterized by the constant sum of the energies of the two protons, they are easily identified in the analyzer spectra by their location in a diagonal band. Cu^{63} (p, pα) events are also energetically possible, and in fact would fall close to the (p, 2p) band, but the use of appropriate degrader foils in front of the counters made it possible to eliminate (p,pα) events from the data, as well as to show that they are rare.

Figure 18-2 shows 2-dimensional analyzer data for a run in which both counters are at 90° to the beam direction. The band corresponding to (p,2p) events is clearly visible; the counts at higher summed energies are accidental events.

The spectrum of events in the band projected onto the energy axis of one counter is a superposition of contributions from both "first" and "second" protons. Because of the constraint that the total energy of the two protons must equal 4.17 MeV, these two spectra (for either counter) are reflection-symmetric about 2.08 MeV. The first and second protons contribute equally to the observed total cross section at 2.08 MeV, although the relative contributions at other energies are not determined without further assumptions.

The strength of gamma competition is arrived at by comparison of the cross section for two-proton events with the single counter cross section, which includes events in which either a gamma or second proton may follow a first proton. The observed result is that gamma competition with 2 MeV protons is very strong;

it is concluded from an analysis outlined below that only about 8% of 2.08 MeV first protons are followed by a second proton.

The analysis proceeds along the following lines: the cross sections required are 1) the total cross section for proton emission at 2.08 MeV and 2) the total cross section for emission of coincident 2.08 MeV protons. The total cross sections should in principle be obtained by an experimental integration over all counter solid angles. If, however, the angular distributions are reasonably isotropic, measurements at a single set of angles suffice. In the present analysis departures from isotropy are ignored. From the single counter experiments it is found that the differential cross section at 105° (lab) for the emission of 2.08 MeV (channel energy) protons is 270 ± 90 μb/sterad MeV. The uncertainty arises primarily from the steepness of the spectrum near 2 MeV, which makes uncertainties in energy calibration and beam energy very important. From the coincidence experiment it is found that the differential cross section for events in which two protons are emitted to the ground state of Ni^{62}, both at 90° and each with an energy of 2.08 MeV, is 3.3 ± 0.7 μb/sterad^2 MeV. The differential cross section measured in this particular geometry is multiplied by 4π to give a figure of 42 ± 9 μb/sterad MeV for the differential cross section of 2.08 MeV protons in one counter coincident with another 2.08 MeV proton. Half of this total is then compared with the single counter result quoted above. With corrections for second protons in the single-counter spectrum, the second-proton cross section is therefore (.085 ± .03) of the cross section for emission of the first proton. Besides the previously mentioned uncertainty, poor statistics in the coincidence experiment contribute most to the uncertainty of the final result.

The outcome of particle-gamma competition depends upon the angular momentum which the particle carries off.[2] Calculations of the angular momentum population of the intermediate nucleus are therefore being made as a prelude to further interpretation of the results. (D. Bodansky, and E. R. Parkinson)

---

1 Cyclotron Research, University of Washington (1963) p. 40.
2 J. Delorme, Nucl. Phys. 47, 544 (1963).

---

19. Gamma Rays from Compound Nuclear Reactions

Alpha particles of 42 MeV energy presumably have a good probability of forming a compound nucleus because of their very short mean free path in nuclear matter. Furthermore, an alpha particle of this energy incident upon a medium-weight nucleus can bring in on the average twelve to fourteen units of angular momentum. Because of the Coulomb barrier for charged-particle emission, the compound nucleus is expected to de-excite mainly by neutron emission, followed by a gamma-ray cascade. In the case of 42 MeV incident alpha particles, the most probable number of emitted neutrons is three.

These neutrons emitted from a compound nucleus are expected to have an evaporation-type energy spectrum where the emission of low-energy neutrons is

strongly favored. Thus, it is not expected that the emitted neutrons will on the average carry away much of the angular momentum. At the end of the neutron cascade the residual nucleus would then be expected to be in a state of fairly low excitation energy but rather high angular momentum.

The purpose of this project is to study what happens at the end of the neutron cascade by studying the gamma-rays that are emitted. This is to be done over a very wide range of nuclear mass and for both deformed and spherical nuclei. The energy distribution of the gamma radiation will be investigated in order to find out the average number of photons emitted and the total amount of energy they carry away per nuclear reaction. The angular distribution will be investigated in order to study angular momentum effects in the decay of the residual nucleus by gamma radiation.

Some work has already been reported by Mollenauer[1] on the investigation of the total amount of energy given off in the form of gamma radiation. One of the great difficulties encountered by Mollenauer was the complex response of a NaI crystal to monoenergetic gamma radiation. This made the unfolding of the spectrum of a broad distribution of gamma rays very difficult. This difficulty has been partially overcome by constructing an anticoincidence annulus spectrometer. This detector and its instrumentation is described in another section of this report.[2] The advantage of the anticoincidence annulus spectrometer lies in its simpler energy response for monoenergetic gamma radiation. This makes the unfolding procedure much easier and much more reliable.[3]

An example of the gamma spectrum obtained from alpha particle bombardment of a heavy nucleus is given in Figure 19-1. It is known from activation studies[4] that the predominant reaction in gold at this energy is the $(\alpha, 3n)$ reaction. Thus it is presumed that most of the gamma radiation is from Tl^{198}, an odd-odd, nearly spherical nucleus. Except for a few discrete lines, the spectrum is almost continuous with few gamma rays emitted with energy greater than 1.5 MeV.

On the other hand the spectra of light nuclei are expected to show discrete lines, possibly superimposed on a continuum, due to the rather wide level spacing. An example of the spectrum obtained from a light nucleus is shown in Figure 19-2. All of the lines in this spectrum can be identified with residual nuclei produced by energetically possible reactions in Al^{27}. It is also seen that there is a very appreciable number of gamma rays emitted with energies above 2 MeV.

The group of nuclei which have been most carefully investigated to date are the rare earths which lead to even-even deformed nuclei by the $(\alpha, 3n)$ reaction. Separated isotopes of these rare earths have been obtained from the Oak Ridge National Laboratory. Unfortunately, these are available only in the form of the oxide powder. Targets are prepared by making a slurry of the oxide powder and polystyrene dissolved in benzene. The slurry, typically 20 mg/cm^2 thick, is placed on a thin nylon backing and allowed to dry.

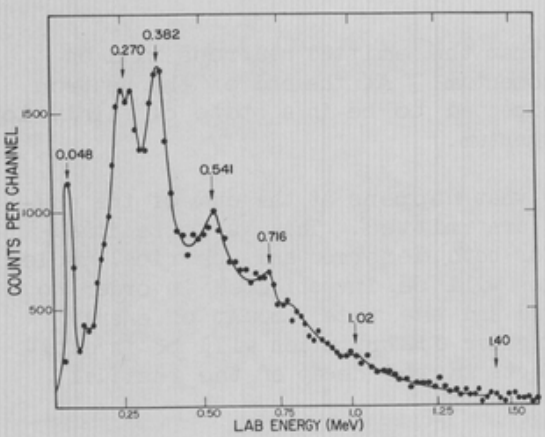

Fig. 19-1 Prompt gamma spectrum from 42-MeV alpha particles on Au^{197}. This spectrum was taken with the anticoincidence annulus spectrometer using a 3-inch by 6-inch NaI(Tl) central detector.

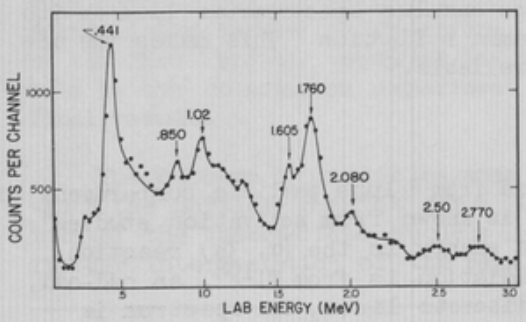

Fig. 19-2 Prompt gamma spectrum from 42-MeV alpha particles on Al^{27}. The spectrometer was the same as in Figure 19-1.

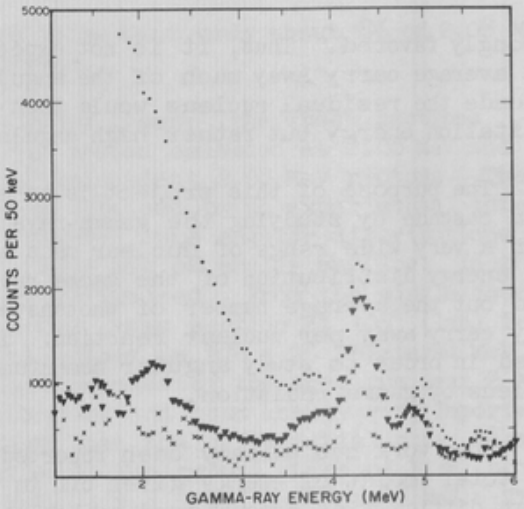

Fig. 19-3 Prompt high-energy gamma spectra from 42-MeV alpha particles on $Gd^{157}_2O_3$ slurry target (····), oxygen gas (xxx), and polystyrene at nylon blank (▼▼▼). The thicknesses of the oxygen and polystyrene + nylon targets were about the same as their respective thicknesses in the $Gd^{157}_2O_3$ slurry target. The spectrometer was the same as in Figure 19-1.

A typical high-energy gamma spectrum from alpha particle bombardment of Gd^{157} is shown in Figure 19-3. The difficulty of having to work with a target containing oxygen, carbon, and nitrogen when studying high-energy gamma rays is strikingly illustrated in this series of spectra. The subtraction of the oxygen, carbon, and nitrogen components in a systematic fashion requires electronic computer techniques, and the necessary programming is now under way. However, it is qualitatively obvious that practically no gamma rays of energy greater than about 3.5 MeV are emitted.

Figure 19-4 shows the low-energy gamma spectrum from the same target. The strong peaks correspond to quadrupole rotational transitions in Dy^{158}.[5] These rotational gamma rays have been observed from many of the even-even deformed nuclei, and many of their energies have been measured.[6,7] The background due to oxygen and carbon is not shown here because in this energy range it is negligible.

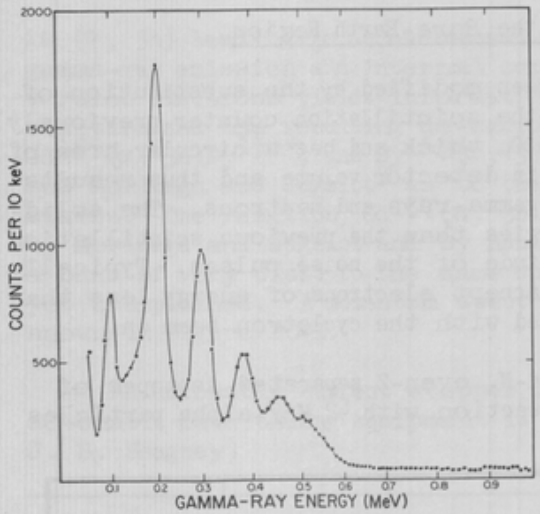

Fig. 19-4 Prompt low-energy spectrum from 42-MeV alpha particles on $Gd^{157}{}_2O_3$ slurry target. This spectrum was taken with the anticoincidence annulus spectrometer using a 1-1/2-inch by 1-inch NaI(Tl) center detector.

Relative intensity measurements are to be made for the lines which can be resolved in an attempt to determine how the rotational levels are being fed. Coincidence measurements are also planned to determine what portion, if any, of the higher-energy spectrum feeds these levels.

It has been shown by De Grout and Tolhoek[8] that in a series cascade such as is the case here, where all the gamma rays have the same multipolarity, that the angular distribution of the first transition is determined by the orbital angular momentum substate population distribution. Furthermore, the angular distribution of radiation emitted in each succeeding step of the cascade is exactly the same as that for the first transition. Angular distributions will thus be measured for each of the observed rotational levels, and coupled with the intensity measurements should give some information concerning the orbital angular momentum substate distribution at the end of the neutron cascade. This substate distribution in the original compound nucleus must be strongly peaked about m=0; so that measurements of the m distribution at the start of the photon cascade gives an indication as to how much the nucleus has been "rocked" by emission of the neutrons. These measurements are now under way, but no final data are yet available. (I. Halpern, E. R. Parkinson, B. J. Shepherd, and C. F. Williamson)

---

1 J. F. Mollenauer, Phys. Rev. 127, 867 (1962).
2 See Section 30 of this report.
3 Cyclotron Research, University of Washington (1963), 20.
4 R. Van de Vijver, Physica 29, 1214 (1963).
5 H. Morinaga and P. C. Gugelot, Nucl. Phys. 46, 210 (1963).
6 G. Bertram, et al., Nucl. Phys. 47, 1 (1963).
7 F. S. Stephens, N. Lark, and R. M. Diamond, Phys. Rev. Letters 12, 225 (1964).
8 S. R. DeGroot and H. A. Tolhoek, Beta and Gamma Ray Spectroscopy (Edited by K. Siegbahn), Interscience Publishers, New York (1955) 613.

---

20. Investigation of Rotational States in the Rare-Earth Region

The toroidal β-ray spectrometer[1] has been modified by the substitution of a surface-barrier solid-state detector for the scintillation counter previously used. This detector, at maximum bias, is 500μ thick and has a circular area of 4.5 cm^2. This is a considerable reduction in detector volume and thus results in a reduction in the background caused by gamma-rays and neutrons. The solid-state detector is also usable at lower energies than the previous scintillation counter because of a reduction in the magnitude of the noise pulses. Typically the discriminator can be set low enough to accept electrons of energy less than 100 kev, and the spectrometer can be operated with the cyclotron beam on.

The targets used to date consist of odd-N, even-Z separated isotopes of gadolinium and dysprosium. The principle reaction with 42 MeV alpha particles

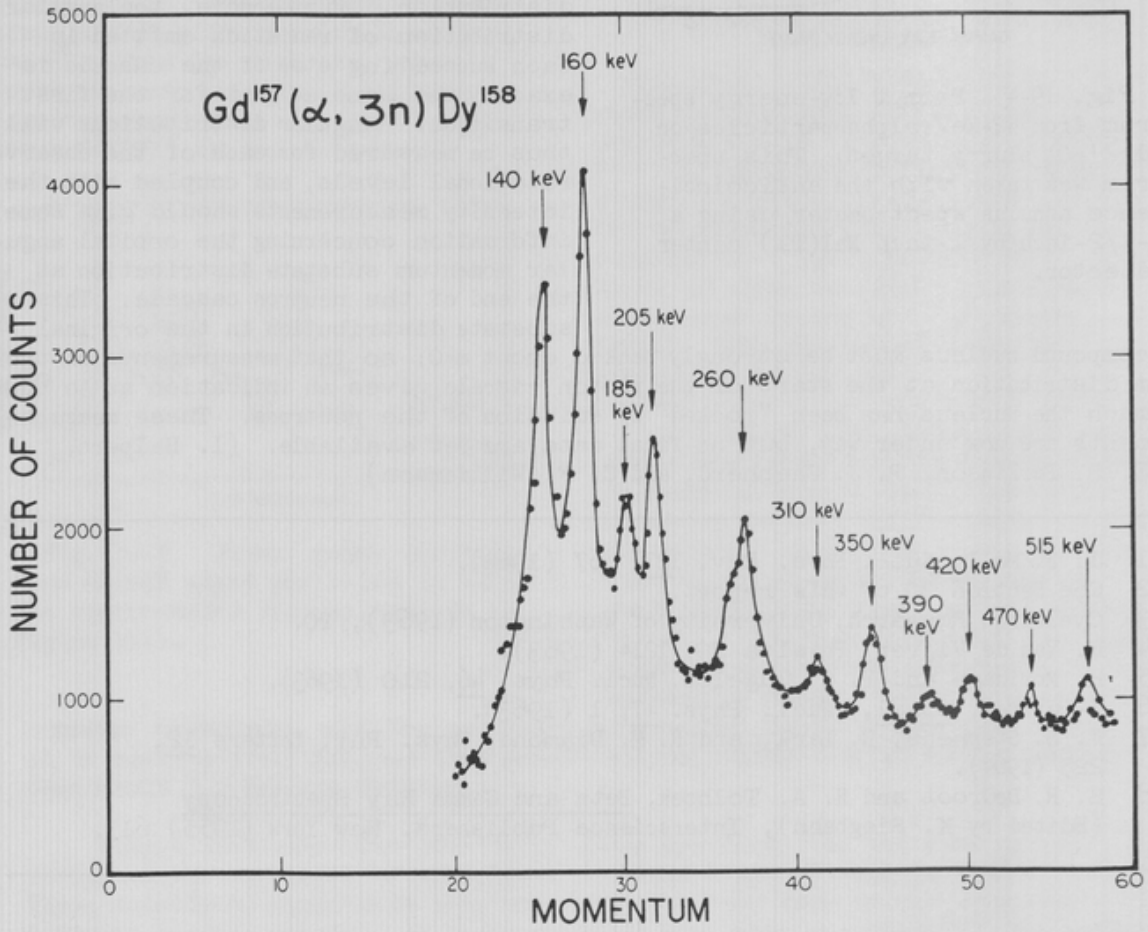

Fig. 20-1 Typical data with time-dependent background subtracted.

is (α, 3n) leading to an even-even nucleus in excited states, which decay by gamma-ray emission and internal conversion. Observation of the internal conversion electrons yields information concerning the levels excited in the reaction and the resulting de-excitation cascade. Two reactions studied, $Gd^{155}(\alpha, 3n)Dy^{156*}$, and $Dy^{163}(\alpha, 3n)Er^{164*}$, confirm the findings of Hansen et al.[2] and Morinaga and Gugelot[3] as to the rotational nature of the low lying excited states. One reaction, $Gd^{157}(\alpha, 3n)Dy^{158*}$, shows the rotational band reported by Morinaga and Gugelot and by Hansen, et al. but in addition there seems to be a band of very close to the same spacing but slightly lower energy which is as yet unexplained. A momentum spectrum of the electrons from this reaction is shown in Figure 20-1.

An automatic current stepper is presently being constructed and more automatic data taking equipment is being contemplated. (J. B. Gerhart and J. S. Heagney)

---

1 Cyclotron Research, University of Washington (1961) 2; (1959) 7; (1957) 2.
2 G. Bertram Hansen, B. Elbek, K. A. Hagemann and W. F. Hornyak, Nucl. Phys. 47 (1963) 529.
3 H. Morinaga, P. C. Gugelot, Nucl. Phys. 46 (1963) 210.

VI. NUCLEAR FISSION

21. (Direct Interaction, Fission) Reactions

A preliminary study has been made of certain (direct interaction, fission) reactions. This study was originally undertaken in order to learn how large a contribution these reactions make to the observed coincidence rates in experiments dealing with charged particle emission during fission.

In these experiments, both 35.5 MeV α-particles and 21.0 MeV deuterons were used to bombard U^{238}. Coincidences between fission fragments and charged particles were measured at a variety of fission fragment and charged particle detector positions. The results of the measurements were consistent with the following assumptions concerning the nature of (direct interaction, f) reactions and charged particle emission during fission:

a. Identity of charged particles.

The charged particles emitted during fission are almost exclusively α-particles, while the (direct interaction, fission) reactions yield both singly and doubly charged particles.

b. Energies of charged particles.

The doubly charged particles which result from (direct interaction, fission) reactions have energies extending from about 20 MeV (the Coulomb barrier height) to about 6 MeV (i.e., a fission barrier height) below the elastic peak whereas the spectrum of the doubly charged particles resulting from charged particle emission during fission peaks at about 15 MeV and is about 10 MeV wide, as in low energy induced fission. Virtually nothing can be said at this time about the spectrum of the singly charged particles resulting from (direct interaction, fission) reactions although these particles are plentiful in the α-particle as well as the deuteron bombardments.

c. Angular distributions of charged particles.

The charged particles from the (direct interaction, fission) reactions are strongly forward-peaked, while the charged particles emitted during fission are as abundant in the back hemisphere as in the front one.

d. Angular correlations between fission fragment and charged particle.

There is a sharp right angle correlation between the fission fragment and charged particle direction of motion in those events in which a charged particle is emitted during the fission process. On the other hand, in (direct interaction fission) reactions, in general no such correlation exists. In (direct interaction, fission) reactions in which charged particles are scattered backward, the angular distribution of

the fission fragments tends to be isotropic. For charged particles which are scattered at right angles to the beam or are scattered forward, the angular distribution of the fission fragments tends to be fore-aft peaked. The axis of symmetry for the fission fragment distribution seems to be the recoil axis in those direct interactions in which a charged particle is scattered at right angles to the beam or into the backward hemisphere.

As has been remarked above, all of the observations so far are consistent within their statistical uncertainties with the foregoing assumptions regarding the nature of the coincident events between fission fragments and charged particles. We are in the process of accumulating enough data to be able to be more sure of the validity of the assumptions and to be able to make reliable estimates of the different differential cross sections. On the basis of the data already obtained for a U^{238} target, it can be said that:

a. Alpha particle bombardments (35.5 MeV)

In the backward direction with the charged particle counter at 135° to the beam and the fission detector at 90° to this counter, the (direct interaction, fission) rate amounts to roughly half of the rate for charged particle emission in fission. Of the direct interaction events seen at this counter configuration, about half involve the emission of singly charged particles, the other half involving doubly charged particles.

b. Deuteron bombardments (21 MeV).

The ratio of (direct interaction, fission) events to those in which charged particles are emitted after fission was compared to the similar ratio in alpha particle bombardment with the charged particle detector at 135°. In the deuteron bombardment the ratio is about four times larger than in the alpha particle bombardments. In this case the direct interaction reactions mostly involve the emission of singly charged particles. (A. W. Fairhall, I. Halpern, and W. Loveland)

---

22. Charged Particle Emission During Nuclear Fission

A set of experiments has been designed to investigate possible dependences of charged particle emission during fission upon the charge and mass of the fissioning species, its excitation energy, its angular momentum, and the relative symmetry of the mass division.

Preliminary data have been obtained in the experiment described in last year's Progress Report.[1] The fission rates in the 42 MeV alpha particle bombardment of U^{238} were measured at 90° to the beam (R_{90}) and at 162° to the beam (R_{162}) and compared with rates, R^{f}_{θ}, measured in the same bombardments, in which a coincidence was required with an α particle emitted at 90° to the fission fragment. For this purpose the α particle counter was placed looking down

upon the (tilted) target at right angles to the beam-fission fragment plane. If the ratio $(R^f_{90}/R_{90})/(R^f_{162}/R_{162})$ differs from unity, it indicates that the fission events which are followed by alpha particle emission differ in some ways from normal fission events. Although the early results seem to indicate a departure of this ratio from unity, the statistical uncertainties are still large but will hopefully be decreased with further data-taking efforts.

Preliminary data have also been obtained in another experiment designed to explore the effect of nuclear angular momentum upon the probability of charged particle emission in fission. A given compound nucleus, Pu^{239}, is formed at an excitation energy, 30.3 MeV, in two different ways (U^{235} + 35.5 MeV α -particles and Np^{237} + 21.0 MeV deuterons). The compound nuclei in these bombardments have different values for their mean square angular momentum (110.3 $\hbar^2$ and 54.8 $\hbar^2$, respectively).[2] The probability of charged particle emission in fission is then compared for the two bombardments.

The experimental method used was essentially the same one used in Reference 1 with the following modifications:

a. The monitoring system to measure the accidental counting rate has been changed to take into account the microtime fluctuations of the cyclotron beam. (See method (b) of Section 27.)

b. Corrections for contributions to the total coincidence counting rate by (direct interaction, f) reactions were made based on assumption (d) outlined in Section 21.

The preliminary results seem to show that the probability for charged particle emission in fission is approximately the same within ±30% for the deuteron-induced fission as compared to the α-particle-induced fission. At this time, the data do not yet permit any definite conclusion to be drawn as regards the effect of nuclear angular momentum upon the probability of charged particle emission in fission. (A. W. Fairhall, I. Halpern, and W. Loveland)

---

1 Cyclotron Research, University of Washington (1963), p. 16.
2 The values for the mean square angular momentum were calculated using the distorted wave code given by R. Bassel, R. Drisko and G. Satchler, "The Distorted-Wave Theory of Direct Nuclear Reactions" ORNL-3240, 1962.

---

23. Capture of 21 MeV Deuterons by Protons

At energies below the threshhold for deuteron breakup, the $d + p \rightarrow He^3 + \gamma$ reaction has been studied by detecting the emitted gamma rays.[1] Two body photodisintegration of He^3, the inverse process of d-p capture, has been studied at higher energies; the angular distribution at 26 MeV[2] and the dependence of the two body photodisintegration at 90° for energies of 8.5 to approximately 100 MeV have been determined.[3] The latter experiments have shown that the Gunn and Irving wave function for the He^3 groundstate[4] yields cross sections that give a good fit to the experimental data.

Measurement of the C. M. differential cross section by detection of the emerging He^3 nuclei in the capture of 21 MeV deuterons by protons was attempted

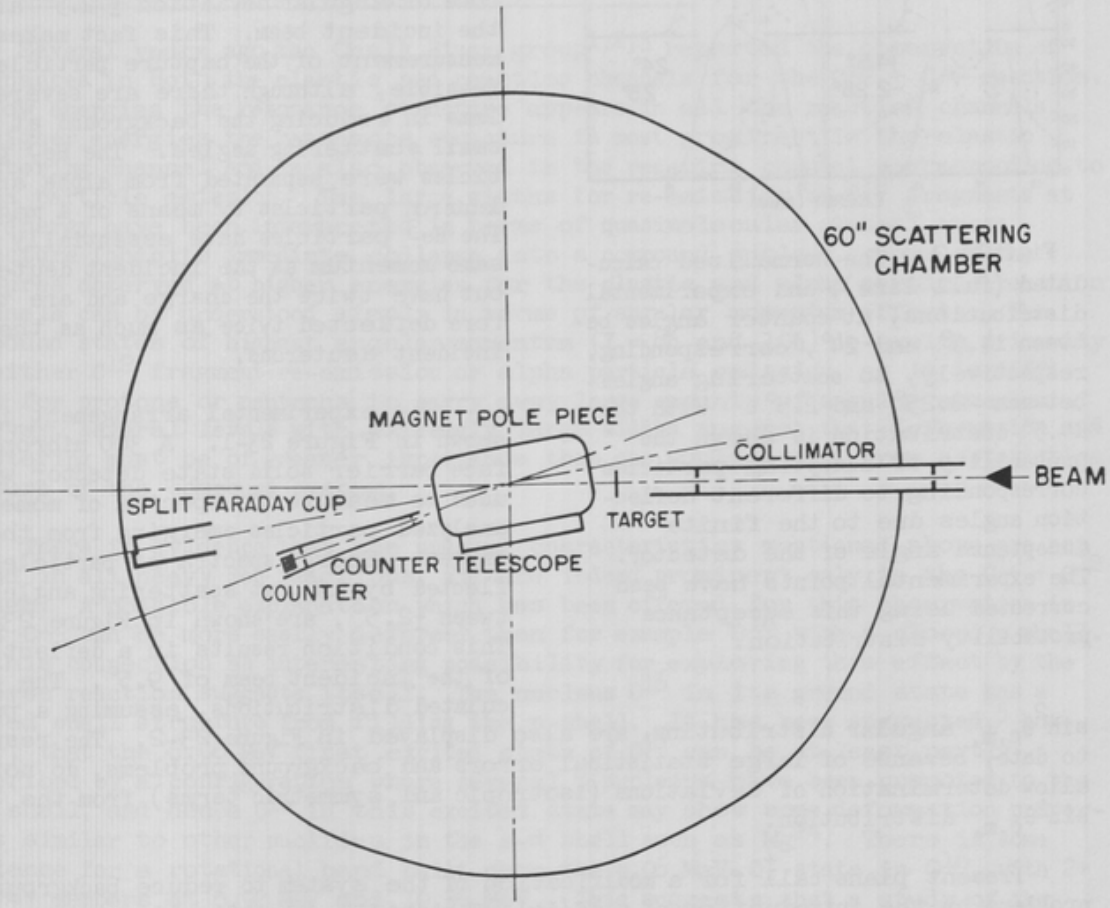

Fig. 23-1 The experimental arrangement.

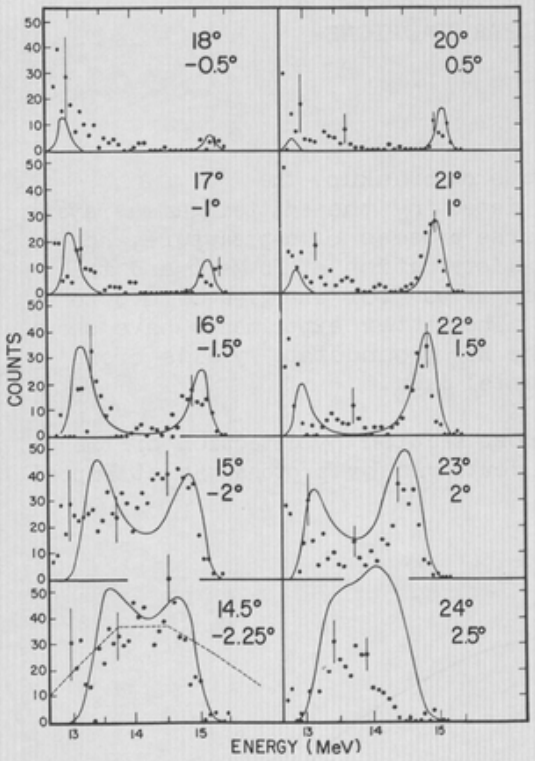

Fig. 23-2 The normalized calculated (full line), and experimental distributions, at counter angles between 14.5° and 24°, corresponding, respectively, to scattering angles between -2.25° and 2.5°. With the 14.5° distribution is shown the probability of accepting particles corresponding to different deflection angles due to the finite acceptance angle of the detector. The experimental points have been corrected using this acceptance probability distribution.

in this experiment. The energy spectrum of particles emerging from the reaction can be used to deduce the differential cross section for the process.[5] This method can be applied to measure the capture cross sections of fast particles by light nuclei,[6] the inverse process of photodisintegration. The energies of particles formed by capture is proportional to the capture cross section as a function of the cosine of the C. M. scattering angle.

The large C. M. momentum and small gamma-ray momentum cause the He^3 nuclei formed in the capture of 21 MeV deuterons by hydrogen to emerge within a narrow cone of angular deviation $\pm$ 2.5° about the incident beam. This fact makes the measurement of the capture particles feasible, although there are severe problems in reducing the background at such small scattering angles. The He^3 particles were separated from alpha and deuteron particles by means of a magnet. The He^3 particles have essentially the same momentum as the incident deuterons, but have twice the charge and are therefore deflected twice as much as the incident deuterons.

The experimental arrangement is shown in Figure 23-1. A 300 micron surface barrier solid state detector was used to measure the spectra of momentum-analyzed particles emerging from the target. Energy spectra of particles deflected by 19°, at scattering angles between $\pm$2.5°, are shown in Figure 23-2. This condition results in a deflection of the incident beam of 9.5°. The calculated distributions, assuming a pure $\sin^2\theta_{c.m.}$ angular distribution, are also displayed in Figure 23-2. The results to date, because of large statistical errors and background problems, do not allow determination of deviations (isotropic and symmetric terms) from the $\sin^2\theta_{c.m.}$ distribution.

Present plans call for a modification of the system to reduce background problems by the introduction of a dE/dx - E particle identification system or by time of flight analysis. Further, refocusing of all capture He^3 particles onto the detector could readily be accomplished by a quadrupole lens pair, since the

particle divergence is small. This addition would greatly simplify measurement and analysis of the data and would very likely give a further reduction in background. (D. L. Hendrie, K. Ilakovac, and E. B. Warren)

---

1 G. M. Griffiths, E. A. Larson, and L. P. Robertson, Can. J. Phys. 40, 402 (1962). Also see earlier references by these authors.
2 L. Cranberg, Bull. Am. Phys. Soc. 3, 173 (1958).
3 B. L. Berman, L. J. Koester, and J. H. Smith, Phys. Rev. 133, B117 (1964); Phys. Rev. Letters 10, 527 (1963).
A. N. Gorbunov and A. T. Varfolomeev, Phys. Letters 5, 149 (1963).
4 J. C. Gunn and J. Irving, Phil. Mag. 42, 1353 (1951).
5 H. H. Barschall and M. H. Kanner, Phys. Rev. 58, 590 (1940).
6 K. Ilakovac and V. Knapp, Nucl. Phys. 43, 69 (1963).

---

24. Investigation of the $Si^{28}(He^4, O^{16})O^{16}$ Reaction

Several years ago the Chalk River group[1,2,3] reported the observation of resonances in both the elastic and reaction channels for the $C^{12} + C^{12}$ reaction. At low energies the resonance structure appears in all the reaction channels. At higher energies the resonance structure is most prominent in the elastic scattering channel and is also observed in the reaction channel corresponding to alpha particle emission. The large widths for re-emission of C^{12} fragments at low energy have been interpreted in terms of quasimolecular states[4] whose structure inhibits immediate collapse into a compound nucleus. Some of the features observed at higher energies for the elastic and alpha particle reaction channels can be understood simply in terms of angular momentum effects. The compound states of highest angular momentum ($I = 8\hbar$ and $10\hbar$) de-excite primarily by either C^{12} fragment re-emission or alpha particle emission, as it is difficult for protons or neutrons to carry away large amounts of angular momentum. However, several levels with extremely large widths suggest that deformation and clustering must be of greater importance than one would expect from a statistical picture of the compound system.

There is evidence that the unusual characteristics mentioned above are not found in all heavy ion reactions, and are indeed prominent only in the $C^{12} + C^{12}$ system. A possible explanation which has been offered for this observation is that C^{12} can be more easily deformed than for example O^{16} with a closed p shell. In this connection an interesting possibility for exploring this effect by the inverse reaction suggests itself. The nucleus O^{16} in its ground state has a closed shell structure from filling the p shell. It has been suggested,[5] however, that the 6.06 MeV first excited state of O^{16} can be at least partly described by a configuration where several p nucleons have been promoted to the s-d shell, and hence O^{16} in this excited state may show some deformation properties similar to other nuclides in the s-d shell such as Mg^{24}. There is some evidence for a rotational band built upon the 6.06 MeV 0^+ state in O^{16}, with 2+ and 4+ members at 6.92 MeV and 10.36 MeV. This suggests that a study of the $Si^{28} + He^4$ system might show a larger cross section for "fission" of the S^{32} compound nucleus into two excited O^{16} fragments than for fission into two O^{16}

nuclei in their ground state. An experiment to test this hypothesis has been initiated.

The experimental approach is as follows. A self-supporting Si^{28} target is bombarded with 42 MeV helium ions. This bombarding energy provides enough energy so that the two O^{16} nuclei can both be formed in their first excited states and still have sufficient kinetic energy to satisfy Coulomb barrier restrictions. The linear momentum brought in by the incident alpha particles results in a forward folding of the coincident O^{16} fragments of approximately 30° for each fragment. Two semiconductor detectors at the appropriate laboratory angles measure the energies of the coincident fragments. The two energies are recorded simultaneously with a 32 x 32 channel analyzer. The primary technical problem is the identification of O^{16} fragments in the presence of protons and alpha particles which are more numerous by many orders of magnitude. The O^{16} fragments have a shorter range for a given energy than do the lighter particles. Pulse shape discrimination[6] against those particles whose range exceeded the depletion depth of the detectors has been successful for separating high energy oxygen ions corresponding to forming O^{16} in its ground state. For the lower energy oxygen ions expected for O^{16} formed in its excited state, particle identification by pulse shape discrimination has not been achieved. Future experiments with a thin, transmission-mounted detector backed by an anticoincidence counter should enable identification of the low energy oxygen ions of short range. Preliminary results indicate that the fission cross section for producing both O^{16} fragments in their ground state is less than 10 microbarns per steradian at 90° in the C. M. system. No results for formation cross sections of O^{16} in excited states have been obtained as yet. (C. J. Bishop, D. Cooke, C. T. Ratcliffe, and R. Vandenbosch)

---

1 E. Almquist, D. A. Bromley, and J. A. Kuehner, Phys. Rev. Letters 4, 515 (1960).
2 D. A. Bromley, J. A. Kuehner, and E. Almquist, Phys. Rev. Letters 4, 365 (1960).
3 E. Almquist, D. A. Bromley, J. A. Kuehner, and B. Whalen, Phys. Rev. 130, 1140 (1963).
4 E. W. Vogt and H. McManus, Phys. Rev. Letters 4, 518 (1960).
5 A. Bohr and B. R. Mottelson, private communication.
6 Cyclotron Research, University of Washington (1963), p. 41.

VIII. ACCELERATOR RESEARCH AND DEVELOPMENT

25. Van de Graaff Accelerator Program

The Van de Graaff Building has been completed and turned over to the University for occupancy by the Nuclear Physics Laboratory. The administrative, shop, and other general laboratory use areas have been furnished and equipped and are now occupied by various laboratory groups.

The two-stage tandem section of the University of Washington FN Series Van de Graaff Accelerator was assembled in the High Voltage Engineering Corporation factory and all mechanical and electrical checks performed. The completion of these tests was delayed so much by various manufacturing difficulties that delivery of the machine could not be made by the date specified in the purchase contract. In view of the performance of the first two FN series machines and in order to eliminate still more delay in shipment and installation, all factory beam tests on the tandem section of the University of Washington machine were dispensed with. These tests will now be made after installation in the Nuclear Physics Laboratory.

Disassembly and shipment of the machine was started in early April and assembly in the Laboratory will start as soon as the tank, which is now in transit, arrives and is set in place in the Laboratory.

Installation of some of the auxilliary equipment such as the insulating gas storage and handling equipment, cooling system piping, and basic power and control wiring has already been started by the Laboratory mechanical and technical staff.

The injector stage of the machine is now being assembled in the factory, but completion and testing will depend somewhat on results of the tests on the three-stage EN series machine for the University of Pittsburg. Delivery of the injector stage is, however, still scheduled for November, 1964. (T. J. Morgan)

26. Van de Graaff Beam Optics Calculations

The beam spot sizes expected at the various targets were calculated by tracing rays from the exit of the accelerator to the targets. In the University of Washington Van de Graaff system the beam emerges from the final accelerator stage and passes through a set of two quadrupole lenses which focus it on a defining slit. Beyond this slit the beam enters the analyzing magnet which bends the beam through a 90° angle and focuses it on the beam energy regulating probes. These probes sense whether the beam is being bent through more or less than 90 degrees by the analyzing magnet, and then they actuate servos which adjust the accelerating voltage to correct the beam energy to the value to which the analyzing magnet is set. The beam then passes through a switching magnet which can switch it into the various scattering areas. From this magnet it passes through another set of two quadrupole magnets which focus it on the target. High Voltage Engineering Corporation furnished calculations for the external beam of an

accelerator similar to that being installed here, but our Van de Graaff accelerator will have the switching magnet 12 inches further downstream from the energy correcting probes, and it has two more scattering areas for the beam to be switched to. Thus it was necessary to calculate the best location for the quadrupole magnets that focus the beam onto the target and to calculate the size of the beam spot on the target.

These calculations were made using matrices furnished by High Voltage Engineering Corporation. These 2 by 2 matrices effect a transformation of the angle and off-axis position of a ray at one point along the optical axis to its angle and off-axis position at another point along the axis. The matrices for the quadrupole magnets were derived by considering the quadrupole lenses as two thin lenses, since any compound lens system is equivalent to two thin lenses located at its principle planes. Viewed in one plane including the optical axis the first of these is a diverging lens, the second a converging lens. In the plane perpendicular to this plane and also including the optical axis, the first lens converges and the second diverges. The result is a net converging of rays to the same focus in both planes if the focal lengths of the thin lenses are adjusted correctly. The small-angle thin lens formulae are used to obtain the transformation. These should give excellent results for this system, since the largest angles involved are about 2 degrees. If one assumes that the quadrupole lens sets have no serious astigmatism and that their principal planes have been located correctly, these calculations should be quite accurate for monoenergetic beams. Although we are able to correct the beam spot size for spreads resulting from spreads in beam energy, we were unable to determine the exact energy spread to expect. For a momentum spread $\Delta P/P = .00025$, the figure used in High Voltage Engineering Corporation's calculations, the spot size is approximately doubled in the horizontal direction, while the vertical direction is unaffected.

The placement of the quadrupole lenses was limited by the divergence of the beam. We would have liked to place them further downstream, but we were limited because the beam could not be allowed to become wider than the inside diameter of the lenses. The beam spot sizes resulting from our calculations are the following:

Beam tube position relative to original beam axis:	Beam spot width (at target) in inches:	Beam spot height (at target) in inches:
45°	0.12	0.19
30°	0.12	0.15
15°	0.13	0.15
0°	0.14	0.15
-30°	0.13	0.18
-45°	0.12	0.19

These figures result from the values for the off-axis position and angular divergence of the beam at the tank exit given by High Voltage Engineering Corporation. Whether these are maximum values or average values is not clear in their report. Thus these values should be considered only estimates on beam spot size, not exact predictions. (T. Hayward and D. Storm)

27. Micro Time Scale Fluctuations in the Cyclotron Beam

In many low counting rate coincidence experiments, it is essential to know fairly accurately the number of accidental or chance coincidences that have occurred during any given data collection period. These accidental coincidences are the result of two uncorrelated events which occur in one's detection apparatus within the resolving time of the coincidence circuitry. Quite frequently, the number of accidental coincidences which have occurred in a given experiment is estimated by statistical considerations based on the assumption that the number of ions per cyclotron beam burst is constant from one beam burst to another. Recent observations[1] have shown that this assumption may not be valid--at least for the University of Washington cyclotron. Therefore the following measurements were undertaken to determine the extent of the micro time scale fluctuations in the cyclotron beam, and, if possible, to eliminate these fluctuations. The experiment was carried out in the sixty-inch scattering chamber. Two methods were used:

a. Direct Method.

The intensities of a sequence of beam bursts were observed by placing a thin plastic scintillator in the cyclotron beam and observing the light output with a photomultiplier tube. The scintillator was a 0.002-inch thick N.E. 102 (Nuclear Enterprises) and the photomultiplier tube, an RCA 6810A, was situated about 18 inches away from the scintillator. A calculation demonstrated that the statistical uncertainty in the number of photons observed in each burst was insignificant, and it was experimentally determined that none of the pulses was saturated; thus the observed pulse amplitudes were proportional to the number of particles passing through the scintillator. These pulses were observed as a function of time on randomly-triggered single-sweep traces of an oscilloscope. It was easy to determine the distribution of intensities of successive beam bursts from photographs of such oscilloscope traces.

b. Indirect Method.

Two semiconductor radiation detectors were used to observe beam particles which were elastically scattered from a heavy element target. If the pulses from the two detectors are in time coincidence, then such coincidences are necessarily accidental. In one version of the method, a fast slow coincidence system was used to compare (accidental) coincidence rates when the pulses from the counters were associated with the same beam burst with the rates observed when the pulses were associated with different beam bursts. Both sets of rates were simultaneously measured, the latter set with a delay equal to an integral number of cyclotron periods inserted into one of the counter lines to its coincidence input.

In the other version of this method, the pulses from the two detectors were used to respectively start and stop a time-to-pulse-height converter. The analyzed output of the converter showed maxima

whose separation in time corresponded to the cyclotron period, as expected. In a single run it was possible to observe accidental rates associated between overlaps of cyclotron bursts spaced n periods apart where n ranged from zero to about ten.

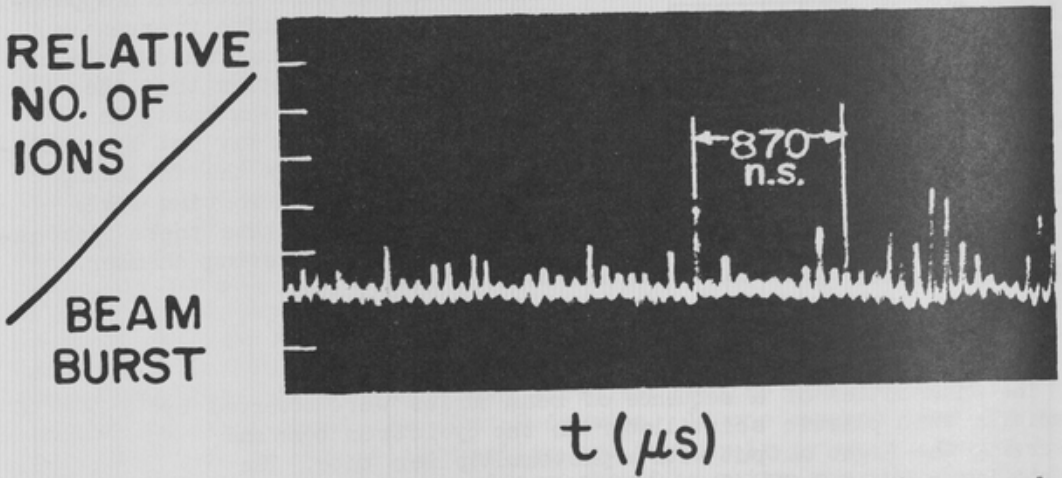

Fig. 27-1 The number of ions per beam burst as measured for several beam bursts by method (a). Each little spike represents one beam burst.

Figures 27-1 and 27-2 show the results of measurements by methods a and b respectively. Figure 27-1 shows a typical sequence of beam bursts. The results obtained with method b (Figure 27-2) can be interpreted with the aid of Figure 27-3. If all cyclotron beam bursts were of equal intensity, the pattern one would see in Figure 27-2 would be as in Figure 27-3a with all peaks equal in height. If the beam bursts were not all equal in intensity and randomly distributed in time, the pattern would be as in Figure 27-3b where the zero delay peak exceeds all of the others which are uniform. The ratio of the zero delay peak to the large delay peaks is just $\overline{I^2}/\overline{I}^2$ where I is the intensity of a beam burst. It is important to remark here that if this ratio is measurably larger than unity, it means that some of the beam bursts must be rather huge compared to the average. If, for example, the I's are distributed uniformly from I = 0 to some maximum I_m, then it can easily be shown that the ratio $\overline{I^2}/\overline{I}^2$ is only 4/3. For a ratio as large as that in Figure 27-2 (about 5), some bursts must be unusally large. The curve with a gradual instead of a discontinuous fall-off from the central peak (Figure 27-3c) arises if there is a correlation in magnitude between successive beam bursts. The following conclusions were drawn from the experiment. (All methods of measurement gave results that agreed within their experimental uncertainties):

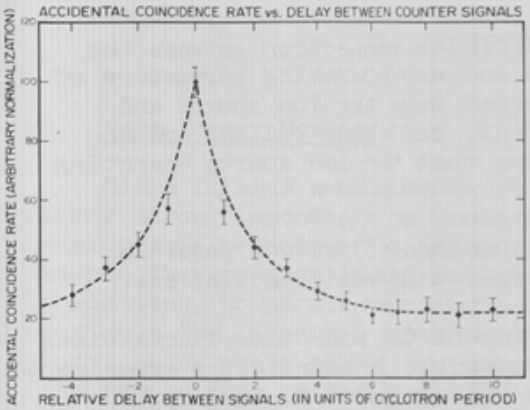

Fig. 27-2 The accidental coincidence rate between two signals from uncorrelated events as a function of delay between the signals. The dashed curve gives the expected rates on the basis of the following simple model. A fraction (22%) of the time there is a cyclotron beam burst of constant height. The remaining bursts are of zero intensity. The time distribution of zero and full intensity bursts is random except that a full burst has a 65% (instead of the average 22%) chance to follow a full burst.

a. For usual cyclotron operating conditions, $\overline{I^2}/\overline{I}^2$ is close to unity and the fluctuations in ions per beam burst are relatively small. But occasionally there are severe fluctuations like those illustrated by Figures 27-1 and 27-2.

b. The distribution of the uneven beam bursts seems to be essentially random in time except for a moderate correlation between succeeding bursts. The correlation time implied by Figure 27-2 is of the order 0.1 μs. Any mechanism invoked to explain the micro-time fluctuations must be consistent with this short time.

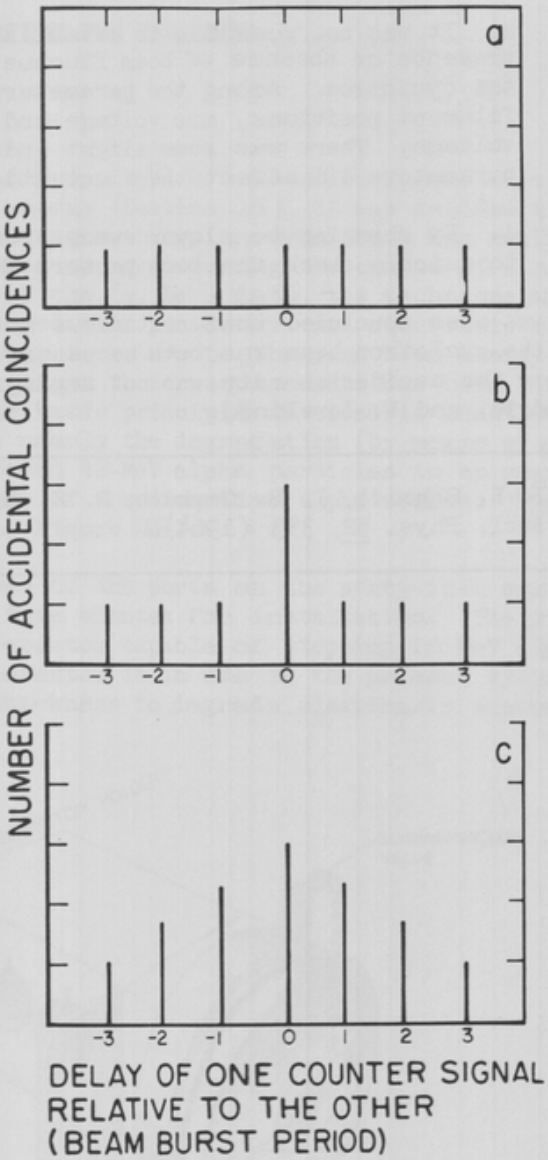

Fig. 27-3 An idealized version of Figure 27-2 for three different situations: a. When all beam bursts are of equal intensity. b. When beam bursts are of unequal intensity and random in time. c. As in b, except that there is a correlation such that large bursts tend to follow large bursts.

c. It was not possible to establish a definite connection between the presence or absence of beam fluctuations and any operating parameters of the cyclotron. Among the parameters checked were the ion source and filament positions, arc voltage and current, deflector voltage and dee voltage. There was some slight indication that the ion source operating parameters did affect the fluctuations.

d. By changing to slower sweep speeds in method (a) it was possible to quickly check the beam pattern for slower time scale modulations.

It was also concluded that continuous monitoring of the microtime fluctuations in the cyclotron beam was both necessary and possible in coincidence experiments where the accidental rate was not negligible. (I. Halpern, J. Heagney, D. Hendrie, and W. Loveland)

---

1 F. H. Schmidt, J. B. Gerhart, R. E. Brown, and W. A. Kolasinski, Nucl. Phys. 52, 353 (1964).

IX. INSTRUMENTATION FOR RESEARCH

28. Beam Energy Monitor

Since initial measurements on the O^{16} (α, Be^8) C^{12} reaction suggested a rather strong dependence on bombarding energy (Section 15), it was decided to develop some technique for monitoring the beam energy in order that one could be assured that no significant energy changes occurred during the course of a run. In addition, to permit reproducibility of the (α, Be^8) data, the technique should provide a "bench mark," independent of cyclotron parameters and electronic settings, which would enable the experimenter to return to the same beam energy from run to run. A simple device which meets these requirements has been built and tested and is currently in use. The basic principle involved is identical to that employed by Benveniste et al.,[1] namely the degradation (by means of a suitable absorber) of elastically scattered 42-MeV alpha particles to an energy that can conveniently be compared to that of a radioactive alpha source. The main features of the device are shown in Figure 28-1.

The unit is designed to fit into one of the ports on the sixty-inch scattering chamber and requires approximately five minutes for installation. The principal components are: 1) solid state detector capable of stopping 10 MeV alpha particles (an Oak Ridge 300 micron SB detector is in use in the present system); 2) an aluminum absorber of sufficient thickness to degrade elastically scattered

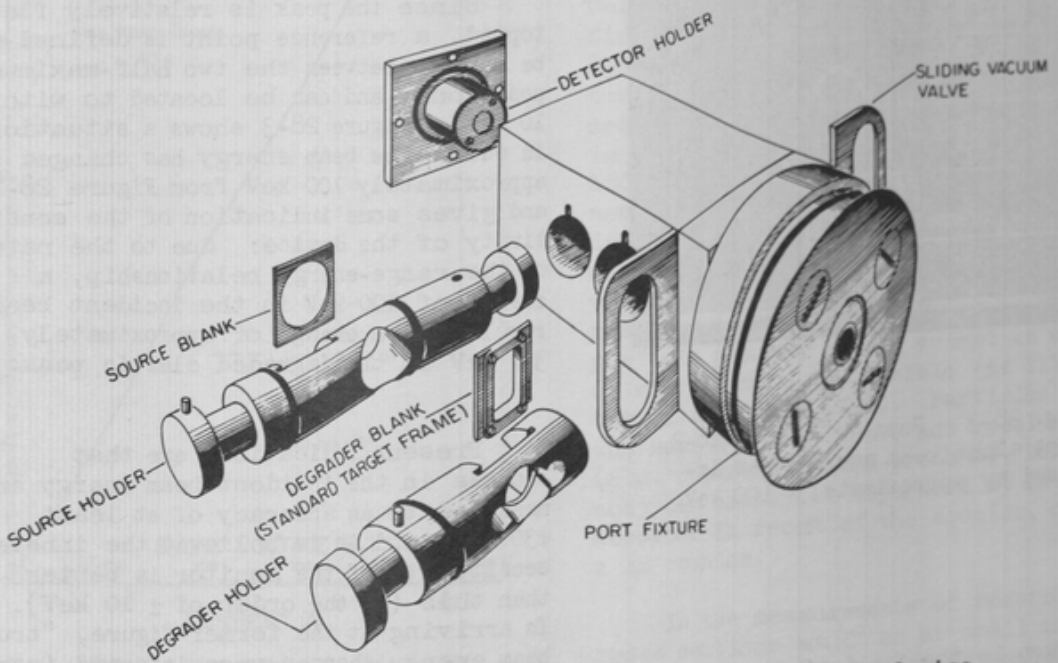

Fig. 28-1 Pictorial view of beam energy monitoring device.

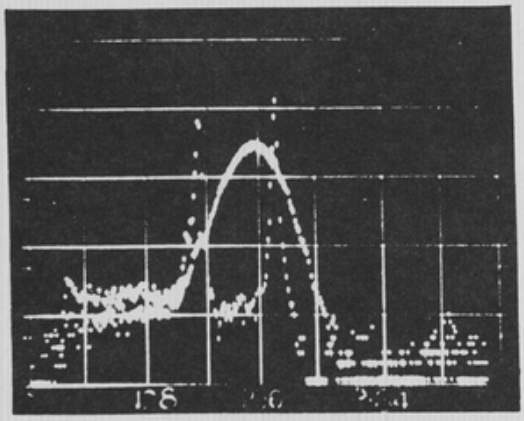

Fig. 28-2 Spectrum of degraded elastically-scattered alpha particles overlapped with radioactive alpha source spectrum.

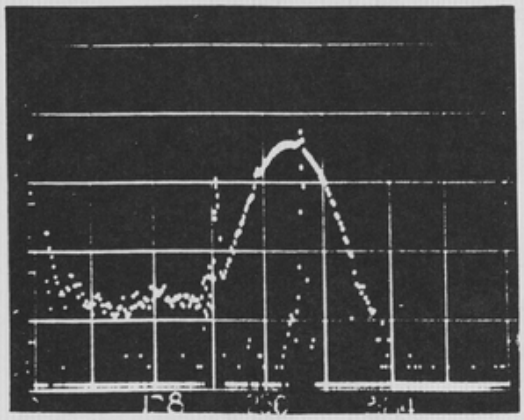

Fig. 28-3 Same as Figure 28-2, except alpha beam energy has increased by approximately 100 keV.

42-MeV alpha particles to 6 - 10 MeV; 3) a source of alpha particles of known energy, conveniently supplied in this case by the laboratory's source maker (E_α = 6.16, 8.78 MeV). The usual procedure has been to first install the unit in the 30° port on the scattering chamber, insert the alpha source and absorber, and then rough the system down with a small fore pump (the sliding valve permits one to isolate the unit from the scattering chamber). Signals from the detector are fed into a 512 channel analyzer, which can then be calibrated using the known energies of the source alphas. When the scattering chamber has been evacuated and beam established, the sliding valve is opened and the foreline closed off. A gold target (1.2 mg/cm^2) is next inserted, and a short run taken. Figure 28-2 shows the degraded elastic peak obtained in this fashion overlapped with the alpha source spectrum.

Since the peak is relatively flat-topped, a reference point is defined to be midway between the two half-maximum positions, and can be located to within 10 keV. Figure 28-3 shows a situation in which the beam energy has changed by approximately 100 keV from Figure 28-2, and gives some indication of the sensitivity of the device: due to the nature of the range-energy relationship, a change of 100 keV in the incident beam results in a change of approximately 350 keV in the degraded elastic peak.

Present indications are that changes in the incident beam energy are measured to an accuracy of at least ±30 keV, and it is believed the inherent sensitivity of the monitor is better than this (on the order of ± 10 keV). In arriving at the former figure, "true" beam energy changes were inferred from changes in the field of the analyzing magnet. A recent run made with the heavy-particle spectometer showed that this method could be in error by as much as 50 keV for a 500 keV charge in beam energy, possibly because of the relatively

large collimators used (1/8 by 3/32 inch). (C. D. Kavaloski)

1 J. Benveniste, A. Mitchell and R. Thomas, Nucl. Instr. and Methods 23, 349 (1963).

29. Construction and Performance of the 1-7/8 by 8-Inch Magnet with a 5/8-Inch Gap

A small magnet (106 lb) was made to be used inside the 60-inch scattering chamber, either on the table or on the arms. The purpose was twofold: (1) observation of nuclear reactions at 0°, and (2) as a Br - E particle identification system.

The magnetic field as a function of current and voltage across the present shunt (11.5 mΩ) is shown in Figure 29-1. The field is very closely linearly dependent on the current, with a residual field of 40 gauss; it is homogeneous to better than 0.25% on the middle line along the gap, between points 1 inch from either side, but the field at these points is 1% lower than in the middle of the magnet, at a field of 10,000 gauss (the highest for continuous running). Deflection of various particles with a field of 7550 gauss is shown in Figure 29-2. The detector (solid state detectors were used for accurate energy measurements) and collimator were placed in a steel shield upon a rotating table and mounted on the scattering chamber arm. The arm and the guide position determine the scattering and deflection angle accepted by the collimator. A very crude resolution in momenta is needed (and desired) to separate the particle groups, and to accept as wide an energy range as possible (as illustrated in Figure 29-2). Particles of the same Z^2/M ratio are not resolved (e.g. α particles and protons), but they can easily be separated by an absorber in front of the counter, or by a ΔE counter.

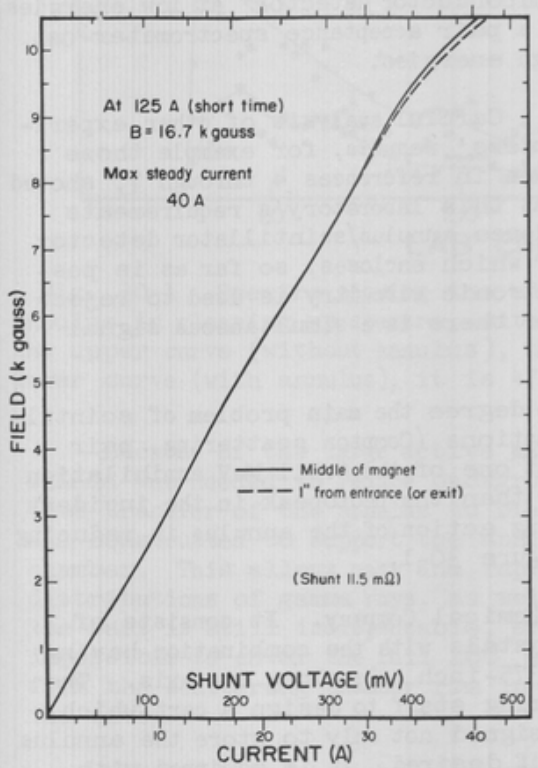

Fig. 29-1 Magnetic field as a function of current and shunt voltage.

In the measurements of reaction cross sections at 0° or at small angles, the main beam also passes through the magnet, and is deflected. A small double-electrode Faraday cup ("split

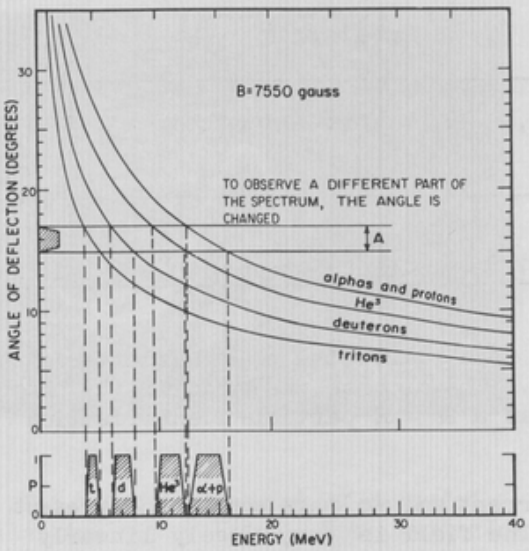

Fig. 29-2 Deflection of p, d, t, He^3 and α particles as a function of energy. Probability of reaching the counter, P, for an assumed angular acceptance of the counter, A, is illustrated.

F.C."), shielded in a block of steel, and was made to integrate the main beam (sum of currents), and to assure a constant deflection in the magnet (by keeping a constant ratio of currents). (K. Ilakovac)

30. Anticoincidence Annulus

Investigations of gamma-ray spectra in this laboratory made apparent the desirability of a more efficient detector, having a high photofraction. This is especially important in the study of relatively featureless spectra and/or spectra above 2 MeV. High resolution can be obtained, at the penalty of low efficiency, by use of a bent crystal spectrometer[1] or lithium-drifted semiconductor detector[2] at low energies, or a pair acceptance spectrometer[3] at high energies.

Careful analysis of other experimenters' results, for example those given in references 4 through 7, showed that this laboratory's requirements would best be met by means of an anticoincidence annulus/scintillator detector system. The annulus is a secondary detector which encloses, so far as is possible, the primary (central) detector. Electronic circuitry is used to reject any signal from the central detector whenever there is a simultaneous signal from the annulus.

The annulus overcomes to a considerable degree the main problem of scintillation detectors, namely that partial interactions (Compton scattering, pair production with subsequent escape of at least one of the 0.511 MeV annihilation quanta) create a tail of pulse heights lower than the photopeak in the incident spectrum. The effectiveness of the guard ring action of the annulus in reducing this low tail in the spectrum is shown in Figure 30-1.

The annulus was obtained from Harshaw Chemical Company. It consists of two optically-coupled NaI(Tl) cylindrical crystals with the combination having an 8-inch diameter, 12-inch length, and a 3.375-inch hole along its axis. The four-month delivery time enabled our engineering staff to design a cart which was fabricated by the shop. This cart is designed not only to store the annulus but also to support it during an experiment if desired. It is equipped with reference arms that bear against the rim of the scattering chamber and position the annulus accurately in angle. The cart also can be positioned vertically with jacks which have ball casters mounted on the ends for final lateral adjustment.

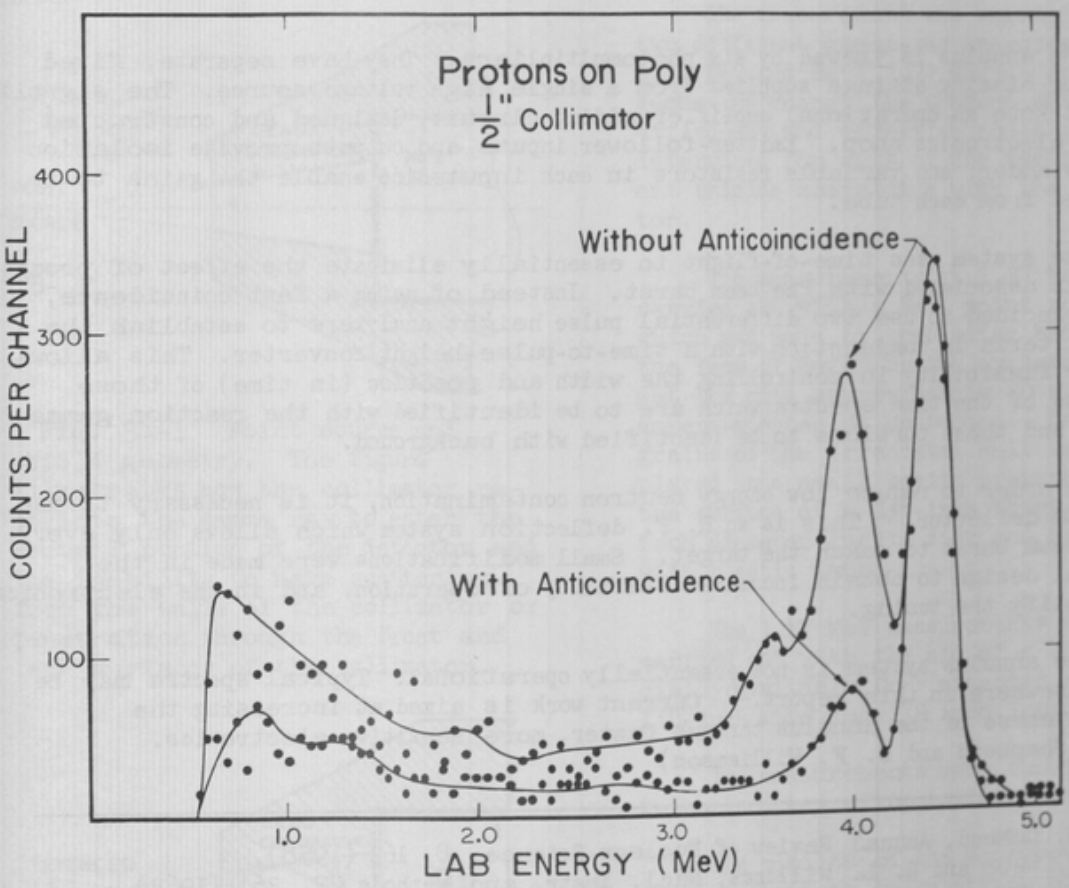

Fig. 30-1 Spectra showing the effectiveness of the anticoincidence annulus in cleaning up spectra, without decreasing photoefficiency. In the upper curve (without annulus), the photofraction is 23.5%; in the lower curve (with annulus), it is 47.7%.

Because of the large active mass of the annulus, a 2.5-inch thick lead shield was needed to reduce background. The shield was made compact, to facilitate transfer of the annulus to other supporting devices. A table was designed and constructed to support the annulus on the rim of the sixty-inch scattering chamber. This allows easy and rapid changes in angle in studies of angular distributions of gamma rays, as well as highly accurate positioning. However, the cart is still indispensable, even when the table is used, because it is impossible to cover the full 180° without removing the annulus and the table from the scattering chamber rim in order to reposition existing equipment in the cave.

Special bases have been constructed to allow the use of NaI(Tl) primary detector crystals of the following dimensions: 3-inch diameter and either 3-inch or 6-inch length, and 1.75-inch diameter and 1.75-inch length. The base-crystal assemblies all have maximum diameters to allow their insertion into the central hole of the annulus. It is also possible to change the type of photomultiplier tube used, if desired.

The annulus is viewed by six photomultipliers. They have separate, fixed resistor biasing strings supplied from a single high voltage source. The signals are fed into an operational amplifier adding circuit, designed and constructed by the electronics shop. Emitter-follower inputs and outputs provide isolation for the adder, and variable resistors in each input line enable the gains to be balanced from each tube.

The system uses time-of-flight to essentially eliminate the effect of prompt neutrons associated with the beam burst. Instead of using a fast coincidence,[8] it was decided to use two differential pulse height analyzers to establish the time criteria in conjunction with a time-to-pulse-height converter. This allows greater flexibility in controlling the width and position (in time) of those portions of the time spectra which are to be identified with the reaction gamma events and those portions to be identified with background.

In order to reduce low energy neutron contamination, it is necessary to use the beam deflector.[9] This is an R. F. deflection system which allows only every third beam burst to reach the target. Small modifications were made in the physical design to obtain increased stability of operation, and in the electronics to simplify the tuning.

The annulus system is now essentially operational. Typical spectra may be seen elsewhere in this report.[10] Current work is aimed at increasing the effectiveness of the annulus through faster, more sensitive electronics. (B. J. Shepherd and C. F. Williamson)

---

1 W. M. DuMond, Annual Review of Nuclear Science, 8, 163 (1958).
2 P. P. Webb and R. L. Williams, Nucl. Instr. and Methods 22, 361 (1963).
3 B. Ziegler, J. M. Wyckoff, and H. W. Koch, Nucl. Instr. and Methods 24, 301 (1963).
4 R. D. Albert, Rev. of Sci. Instr. 24, 1096 (1953). This is of historical interest.
5 C. C. Trail and S. Raboy, Rev. of Sci. Instr. 24, 1096 30, 425 (1959).
6 C. O. Bostrom and J. E. Draper, Rev. of Sci. Instr. 32, 1024 (1961).
7 G. Busuoli, C. Melandri, O. Rimondi and B. Righini, Nucl. Instr. and Methods 22, 324 (1963).
8 R. J. Scroggs, W. Zobel, and F. C. Maienschein, IEEE Trans. Nuc. Sci., NS 11, No. 1 365 (1964).
9 Cyclotron Research, University of Washington (1961), p. 34.
10 See Section 19 of this report.

---

31. Efficiency Measurement of a 4-inch Diameter by 4-inch NaI (Tl) Gamma Ray Detector

An efficiency measurement has been carried out on the 4-inch diameter by 4-inch NaI (Tl) gamma ray detector used in the proton-gamma ray correlation experiments reported earlier.[1] The method used is essentially the coincidence technique described in Reference 2, page 219 ff.

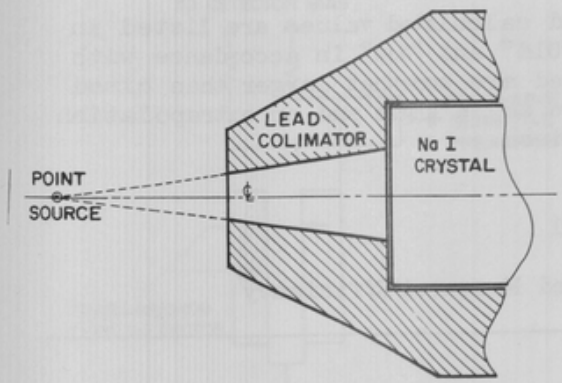

Fig. 31-1 Point source and shield geometry. The figure illustrates how the collimator restricts the gamma ray to enter the central portion of the detector and the inability to have scattering from the walls of the collimator or penetration through the front and back surfaces of the collimator.

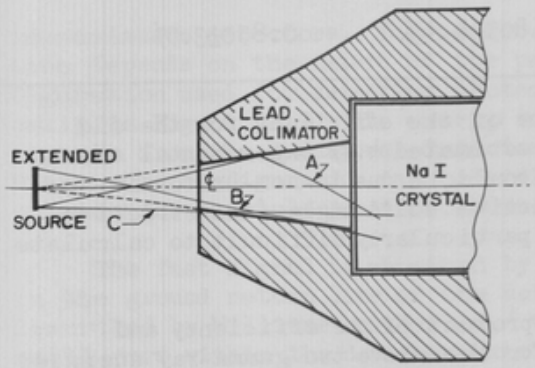

Fig. 31-2 Extended source and shield geometry. The figure illustrates: A. Scattering from side of collimator; B. penetration of back surface of collimator; C. penetration at front surface of collimator.

The measurement was carried out at two different gamma-ray energies (Co^{60} 1.17 MeV and Na^{24} 1.37 MeV). At each gamma-ray energy the product of the efficiency and effective solid angle was determined for each of the two different shields compatible with the detector.

The measurements at 1.37 MeV were carried out with a Na^{24} point source which was made by bombarding Na^{23} (in the form of NaCl) in the cyclotron target box with approximately 30 microampere-minutes of deuterons. Several grains of the irradiated salt were placed in a small cavity prepared on the surface of a 1/8-inch thick, 7/8-inch diameter lucite disk and covered with plastic tape.

The 1.17 MeV measurements were carried out with the aid of a commercially available Co^{60} extended source 1/8-inch wide and 1/2 inch long.

The measurements were carried out to an accuracy of approximately 1.5%.

The results of the measurements were compared to calculations of the efficiency.[3] These calculations are for what is called a broad parallel beam and give only the probability that the incident gamma ray undergoes any interaction with the detecting crystal. This should be quite a good approximation in the case of these measurements where the lead collimator of the shield restricts the beam of gamma rays to enter only the central portion of the detector crystal (Figures 31-1 and 31-2).

In order to carry out the comparison between the observed value of the product of the efficiency and effective solid angle, and the calculations of the efficiency, it is necessary to know the effective solid angle of the detector. This can be calculated rather precisely if the source is a point source (Figure 31-1). However, if the source is an extended source, the calculations become rather complicated. This is due to the fact that gamma rays from the periphery of the source can strike the sides of the collimator and be scattered into the crystal, and they also may penetrate the thin front and back surfaces of the collimator (Figure 31-2).

The comparisons between the measured and calculated values are listed in Table 31-1. The shields have been labeled "Old" and "New" in accordance with their dates of construction. The errors noted are somewhat larger than cited earlier due to uncertainties in the effective solid angle and an extrapolation of the original data required for the comparison

Table 31-1

Comparison of Calculated and Measured Efficiency

	Calculated Efficiency	Old Shield Measured Efficiency	New Shield Measured Efficiency
Na^{24} Point Source 1.37 MeV Gamma Ray	0.840	0.849±2%	0.855±2%
Co^{60} Extended Source 1.17 MeV Gamma Ray	0.861	0.805±4.4%	0.850±3.5%

It will be noted that the measured value of the efficiency for the old shield and extended source lies outside the estimated 4.4% experimental error when compared with calculated values. This could be due to non-uniformity of the source or an incorrect value of the effective solid angle (the effective solid angle of the old shield collimator is particularly difficult to calculate due to the geometry of that shield).

In addition to the measurements of the product of the efficiency and effective solid angle, the spectrum shapes for the above two gamma-ray energies and shields were also determined. (J. B. Gerhart, T. D. Hayward, W. A. Kolasinski, and F. H. Schmidt)

1 Cyclotron Research, University of Washington (1963), p. 14.
2 Beta and Gamma Ray Spectroscopy, Kai Siegbahn, 1955.
3 Efficiencies and Photofractions for Gamma Radiation on Sodium Iodide (Thallium Activated) Crystals, W. F. Miller, John Reynolds and William J. Snow, ANL-5902.

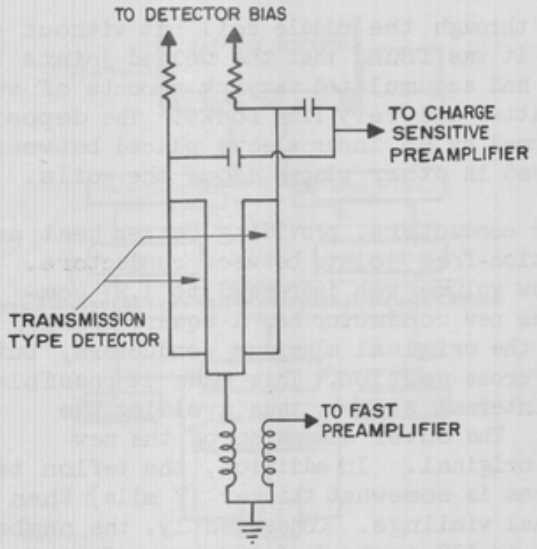

Fig. 32-1 Stacked detector configuration to furnish energy and timing information.

32. Semiconductor Charged-Particle Counter for Fast Coincidence Measurements

Experiments involving measurement of coincidences between charged particles and gamma rays require a particle detection system which, apart from good energy resolution, possesses the following features:

a. Large acceptance aperture to insure reasonable counting rates.

b. A fast rising output signal for forming fast coincidences.

c. Provision for particle identification.

A counter possessing the above features has been developed, incorporating stacked ORTEC RM HJ300 surface barrier transmission detectors. The number of detectors used and the method of connection depends on the nature of the particles studied and their energy. A configuration used for detecting protons up to 10 MeV in energy is shown schematically in Figure 32-1. The energy information is obtained by adding the negative signals from the individual detectors at the input to a charge-sensitive amplifier. The configuration can be modified easily to include more detectors and to provide for particle identification.

The fast signal is obtained by placing a transformer, small ferrite core, in the ground return line of the detectors. A transistor amplifier of the type described by Williams and Neiler,[1] with a rise time of $\approx$ 2 nsec, is mounted on a small card within the detector housing to minimize the pickup of cyclotron noise before the signal is amplified. The output signal typically has a rise time of $\approx$ 10 ns, depending on the detector capacity, and is used to drive a conventional fast coincidence unit. (J. B. Gerhart, W. A. Kolasinski, and F. H. Schmidt)

---

1 C. W. Williams and J. H. Neiler, IRE Trans. on Nucl. Sci., NS-9, No. 5 (1962) 1.

---

33. New Solenoid Windings for the Beta-Ray Spectrometer

Last summer the field coils of the solenoidal beta-ray spectrometer, which carry cooling water as well as current, became plugged by deposits at the joints, which had accumulated during 15 years of use. Every available method was used

to re-establish the flow of cooling water through the middle coil but without any success. When the coils were dismantled, it was found that the welded joints between sections of the aluminum conductors had accumulated varying amounts of what appeared to be a combination of organic matter and very fine rocks. The deposits were concentrated in the constrictions formed by an inner sleeve placed between sections, and almost no deposit was observed in other places along the coils.

New coils have been wound with copper conductors, providing better heat and electrical conductivity and with constriction-free joints between conductors. The ratio of metal to water-carrying hollow volume was increased to 1.27 compared with 1.04 in the original coils. The new conductor has a square cross section with about the same dimensions as the original aluminum conductors, but a cavity with circular rather than square cross section. This made it possible to interlock adjacent pieces, without an internal sleeve, thus avoiding the necessity for constrictions at the joints. The outer dimension of the new conductor is about 5 mils larger than the original. In addition, the teflon tape used for insulation between successive turns is somewhat thicker (7 mils) than the paper tape (5 mils) used in the original windings. Consequently, the number of turns in each layer of the new windings is 130 instead of 132 turns for nearly the same length coil in the original winding. As a result, the field of the compensating coils (which are unchanged) will be stronger than before, for any given field of the main solenoid.

With the original windings removed, it was found that the cylinder on which the coils were wound was out of round by about 100 mils in an over-all diameter of 12.700 inches. This had long been suspected. The bulges were machined off to conform to the depressions. The changed field characteristics resulting from this change probably are the cause of an improved momentum resolution. Though only rough measurements have been made, the momentum resolution for baffle settings which correspond to a theoretical resolution of 1.0% is now observed to be 1.15% instead of 1.45% with the old coils. Because of smooth joints and increased flow of water through the solenoid, cooling is much more effective. For example, at 140 Amperes current, which corresponds to focussed beta particles of about 4 MeV, the rise in temperature is only about 10° C for the innermost coil and about 14° C for the longest, outermost coil. Finally, about 75% less power is required for the transmission of beta particles of the same energy because of lower resistance of cooper windings compared to the original aluminum windings. This combined with better cooling (which means less increase of resistance) have more than doubled the useful range of the spectrometer and D.C. generator system. (J. B. Gerhart and G. S. Sidhu)

34. A Split Faraday Cup for Accurate Beam Positioning and Integration

In many experiments it is undesirable to define the cyclotron beam spot position by collimators because of the high associated neutron and gamma-ray background. However, in many of these experiments it is also desirable to hold the beam accurately centered on the target. In order to meet the needs of these experiments a split Faraday cup system has been installed.

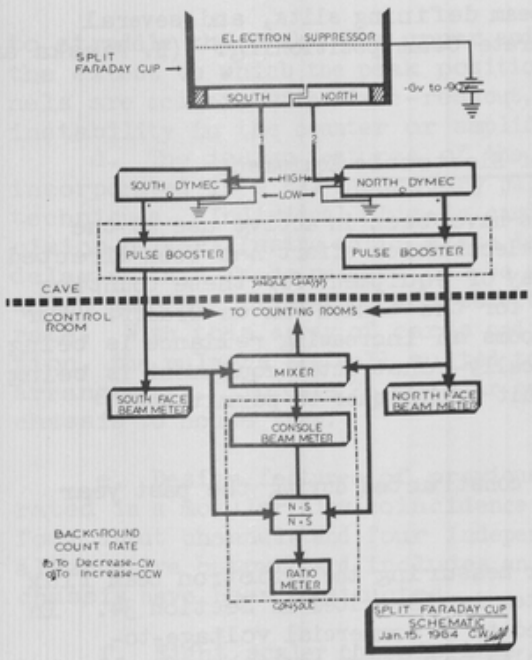

Fig. 34-1 Schematic diagram of split Faraday cup beam positioning and integration system.

The system is shown schematically in Figure 34-1. The face of the Faraday cup is split vertically and the two halves are insulated from ground. Each face of the Faraday cup is connected to the input of a Dymec voltage-to-frequency converter. These integrators are calibrated to one part in 10^5 to give one output pulse for each 10^{-11} Coulomb of charge deposited at the input. The output pulses are boosted in amplitude and fed to the counting rooms and also to the control console. At the console the outputs from the two Dymecs are mixed electronically and also fed to the counting rooms as well as to a precision count rate meter on the console which has been calibrated to read current. A similar calibrated count rate meter is installed in each counting room.

The individual Dymecs are also fed to calibrated count rate meters located in the control room. These measure the current to each face of the Faraday cup and give a visual indication of the balance. If i_s and i_n are the currents striking the two faces of the Faraday cup, it is desired to measure the unbalance U, defined by

$$U = \frac{|i_s| - |i_n|}{|i_s| + |i_n|}$$

A special balance meter circuit has been designed and built which measures log (U) by sensing the difference in analog output between the two count rate meters. The unbalance can be read on a single zero-center meter located on the console which has been calibrated directly in U. The sensitivity of measurement of unbalance is essentially constant over the range of currents from 10^{-6} Amp to 10^{-10} Amp.

Used in conjunction with a fluorescent target and the closed circuit television, this system allows accurate alignment of the beam defining slits. The television target can then be removed and the null maintained by slight adjustment of the analyzing magnet current. The sensitivity of the device allows holding the beam spot position on the target constant to better than ± 1/32".

At the present time the corrections for drift are made manually by the operator. In principle, the error signal from the null meter could be incorporated into a negative feed back loop to give automatic control; however, such a system has not yet been installed. The system has been in operation for several months and appears to be very reliable. It has been extremely useful in

determining the optimum positions for the beam defining slits, and several experiments depend heavily upon it for accurate beam positioning. (H. Fauska and C. F. Williamson)

35. Design, Development and Construction of Electronic Equipment

During the past year two counting rooms have been in active use at the cyclotron, and a considerable share of the electronics effort has been directed toward providing a gradually improving array of equipment for these counting rooms. Two counting areas are also planned for the tandem Van de Graaff. For both cyclotron and Van de Graaff counting rooms an increasing reliance is being placed on commercial electronics units. Locally-constructed equipment is being built, wherever possible, with printed circuit techniques to permit easy duplication as need arises.

Specific items of electronic equipment constructed during the past year include:

a. A new system has been installed for measuring the cyclotron beam flux in scattering experiments. Part of the system is described in Section 34. In the new system the Faraday cup current is fed to a commercial voltage-to-frequency converter with an output of one pulse per 10^{-11} coulombs of collected charge. This output can be scaled to give the total flux. The output can also be fed to a count rate meter to indicate instantaneous beam intensity. Five count rate meter units have been constructed for the latter purpose. In addition a count rate ratio measuring unit has been designed and constructed which compares the currents in the two sections of a Faraday cup (see the discussion of the split Faraday cup in Section 34). Aside from convenience, the present system is preferable to the previous system in that it has less severe problems of cable shielding and the Faraday cup does not develop a significant d.c. voltage as charge accumulates. The calibration remained constant to within 0.002% over a period of 4 months.

b. A three-parameter data recording system has been developed for use in experiments where three pulse heights must be recorded in coincidence. This is accomplished using three analog-to-digital converters, three address scalers, and an 11-digit Hewlett-Packard decimal printer. Existing ADC's were used (one from the Nuclear Data 1024-channel analyzer and two from the locally built 256-channel two-dimensional analyzer). The address scalers use modified versions of our standard 200-kc scaling cards, preceded by several stages of binary scaling. Auxiliary units which were built as part of the over-all system include a dead time device to disable all inputs until the printer is ready to handle the next event, and a marker unit to put special identifying symbols on events (e.g. accidental events, distinguished by their occurrence in a delayed coincidence configuration).

c. A differential monitor unit has been designed and built. This unit is essentially a fast three-channel pulse height analyzer. The width of each channel may be independently controlled by a helipot. The three channels are always adjacent, with no gaps between channels. The unit is designed primarily for monitoring counts in a single peak. Typically the central channel would be adjusted

to straddle the peak. The upper and lower channel rates would then indicate the extent to which the peak position shifted. The outputs of the three channels are scalers with nixie-readout, giving a rapid visual indication of any instability in the counter or amplifier gains.

d. The design features of the previous eight-channel pulser have been incorporated in a new laboratory pulser system based on modular construction techniques. Individual plug-in cards serve as fast pulsers, slow pulsers, precision pulsers (using solid state devices rather than mercury relays), and time delay units. These pulsers can be simultaneously activated by additional cards which generate trigger pulses selected to be either at a random or non-random rate. With this array of cards and the flexibility offered by modular construction, the pulsers are well suited to the checking of complicated electronic arrangements. To date 24 modular cards have been constructed as well as four chassis to house them.

e. Design features of previous slow coincidence units have been incorporated in a modular slow-coincidence chassis. The new unit typically contains four input channels and four independent coincidence output combinations. An alternative output card includes an anticoincidence option. To date two such chassis have been constructed.

f. Eight scaler chassis have been completed, primarily for use with the tandem Van de Graaff. Each chassis contains eight decades, which may be used as a single eight-decade scaler or two four-decade scalers. A timer and master scaler controller has also been built for use with these scalers.

g. Two ovens were built for use in fabrication of lithium drifted solid state detectors. Additional equipment built for this purpose includes two special power supply units for bias voltages, and a metering device for use with a 4-point resistivity probe.

h. A test punch driver unit has been constructed to facilitate maintenance of the paper tape perforators used with our multi-channel analyzers.

i. Additional chassis which have been constructed include: two stretcher chassis for use in x-y particle identification systems, charge sensitive preamplifiers for use with solid state detectors, voltage sensitive preamplifiers for use with photomultiplier tubes, and power supplies for use with solid state detectors.

Equipment purchased commercially during the past year includes: a multichannel analyzer system including a Nuclear ND-120 512-channel analyzer, a Nuclear Data dual amplifier, a Nuclear Data buffer storage unit, a Tally paper-tape punch, a Tally paper-tape reader, a Tally tape-to-typewriter converter, an IBM typewriter, and a Tektronix RM-503 oscilloscope; a Hewlett Packard 50-mc electronic counter; two Dymec voltage-to-frequency converters; a Cosmic coincidence chassis; several preamplifiers for solid state detectors; 3 Ad-Yu 0-110 nanosecond delay line boxes; a Tektronix 541 oscilloscope; 2 Calibration Standard precision voltmeters, a Hewlett Packard decimal printer; a Tektronix operational amplifier plug-in and power rack; 18 relay racks; and a Wang Laboratories angle encoder system for the new 60" scattering chamber. (L. H. Dunning, H. Fauska, R. E. Karns, K. H. Lee, G. C. Monge and N. G. Ward)

36. On-line Computer for Data Handling

A study has been undertaken of computers suitable for on-line data handling in nuclear experiments. Consideration has been given to means of utilizing a computer, the desired capabilities of a computer, and specific programming problems. On the basis of one phase of this study, a proposal for funds has been prepared and submitted to the U.S. Atomic Energy Commission. (D. Bodansky, H. Fauska, J. B. Gerhard, B. J. Shepherd, and R. Vandenbosch)

37. Target Preparation

The targets and techniques listed in tables 37-1 and 37-2 have been prepared in the past year.

Table 37-1

Targets Prepared in the Past Year

Target	Method of Preparation	Backing*	Thickness
Li	vac. evap.	s.s.	1 mg/cm^2
Li_3N	nitriding Li metal foil	Ni, nylon	1 mg/cm^2
LiF	vac. evap.	Ni, nylon	0.1 - 1 mg/cm^2
B	vac. evap.	Ni, Au	1 mg/cm^2
C	carbon arc	s.s.	10 - 100 μg/cm^2
C	painting	s.s.	0.2 - 2 mg/cm^2
TiN	nitriding Ti foils	s.s.	1 - 3 mg/cm^2
NiO	oxidizing Ni foils	s.s.	0.2 - 1 mg/cm^2
Mg	red. of oxide	nylon	$\sim$ 200 μg/cm^2
Mg	vac. evap.	s.s.	0.3 - 1 mg/cm^2
Al	vac. evap.	s.s.	0.1 - 1 mg/cm^2
SiO	vac. evap.	nickel	0.1 - 1 mg/cm^2
CdS	vac. evap.	nickel	1 mg/cm^2

Table 37-1 (continued)

Metallic Halides	vac. evap.	Ni,Au,nylon	0.1 - 1 mg/cm^2
Ca	red carbonate	nylon	~ 200 μg/cm^2
Ca	vac. evap.	s.s.	0.5 - 1 mg/cm^2
V	rolling	s.s.	2 - 5 mg/cm^2
Cr	vac. evap.	s.s.	0.1 - 0.2 mg/cm^2
Cr	electro-deposition	s.s.	1 - 5 mg/cm^2
Fe	electro-deposition	s.s.	1 mg/cm^2 up
Co	electro-deposition	s.s.	1 mg/cm^2 up
Ni	electro-deposition	s.s.	1 mg/cm^2 up
Cu	vac. evap.	s.s.	0.2-2 mg/cm^2
Cu	electro-disposition	s.s.	1 mg/cm^2 up
Nb	rolling	s.s.	3 mg/cm^2
Zn	electro-deposition	s.s.	1 mg/cm^2 up
Cd	electro-deposition	s.s.	1 mg/cm^2 up
Sn	electro-deposition	s.s.	1 mg/cm^2 up
Sb	electro-deposition	s.s.	1 mg/cm^2 up
Rare Earth Oxides	slurry	nylon	1 - 20 mg/cm^2
Ta	rolling	s.s.	5 mg/cm^2
Au	vac. evap.	s.s.	0.1 - 3 mg/cm^2
Pb	vac. evap.	s.s.	0.5 - 2 mg/cm^2
Bi	vac. evap.	s.s.	0.2 - 3 mg/cm^2
Thorium Oxide	slurry	vyns	0.1 - 0.2 mg/cm^2
Uranium Oxide	electro-disposition	Ni	0.1 mg/cm^2

* s.s. indicates self-supporting

Table 37-2

Plating Baths

Target*	Plating Solution	Current Density ma/cm^2	Anode	Cathode	Typical Thickness
Cr	100:1 Chromic acid to sulfuric acid, lower limit 300 mg CrO_3 per 10 ml. solution	250	Pb	Cu	$\geq$ 1 mg/cm^2
Mn	150 g. $MnSO_4$/ℓ 75 g. $(NH_4)_2SO_4$/ℓ 60 g. $(NH_4)CNS$ pH 4.0 - 5.5, temp 25° C	150	Pt	Al	$\geq$ 1 mg/cm^2
Fe	$FeSO_4$ as required sat. $(NH_4)_2C_2O_4$ solution. Prepare by pptng. $Fe(OH)_3$ with NH_4OH from sulfate solution and redissolve hydroxide with just enough oxalic acid solution. pH 6-7	10	Pt	Cu	$\geq$ 1 mg/cm^2
Co	750 mg. $CoCl_2 \cdot 6H_2O$/ 5 ml. H_2O, 900 mg. $CaCl_2$/ 5 ml. H_2O	10	Pt	Cu	$\geq$ 1 mg/cm^2
Ni	$NiSO_4$ as required 20 ml. NH_4OH/100 ml. 1-2 g. $(NH_4)_2SO_4$/ 100 ml.	10	Pt	Cu	$\geq$ 1 mg/cm^2
Cu	2.6 g. $CuSO_4$ 5 ml. H_2SO_4 5 ml. HNO_3 100 ml. H_2O	0.5-2	Pt	Polished steel	$\geq$ 1 mg/cm^2

Table 37-2 (continued)

Zn	$ZnSO_4$ as required 20 ml. NH_4/100 ml. 1 g. $(NH_4)_2SO_4$/100 ml. 1 g. KCN/400 mg Zn	2	Pt	Cu,Au	> 1 mg/cm^2
Cd	$CdSO_4$ as required 1 ml. H_2SO_4/100 ml. H_2O	50	Pt	Cu,Ni, Au	0.2-6 mg/cm^2
Sn	$SnSO_4$ as required 7.5 g. oxalic acid/ 100 ml. 3.3 g. $(NH_4)_2C_2O_4$/100 ml. 1.3 g. hydroxylamine HCl/100 ml.	5	Pt	Cu,Au	0.2 mg/cm^2 up
U	1 mg. $UO_2(C_2H_3O_2)_2$/ ml. 0.4 M $(NH_4)_2C_2O_4$ pH 5, temp. 80° C	130- 150	Pt	Ni	100 µg

* All with the exception of uranium can be made self-supporting by chemically removing the backing.

The apparatus used for vacuum evaporation is a CVC LC1-14B laboratory system with an ultimate vacuum of 2×10^{-7} mm Hg. Heavy copper electrodes are used. In the near future an electron gun will be installed allowing greater flexibility in target materials.

The electroplating procedure was used mainly to prepare foils of isotopes which are available in limited quantities and also to prepare thicker foils of the transition elements which alloy with tungsten when molten and cannot be prepared by vacuum evaporation.

Only the more interesting or non-standard techniques will be described in more detail.

Nitrogen

Natural or monoisotopic nitrogen foils are made by heating titanium foils to approximately 1200° C with an induction heater in a closed quartz system containing nitrogen for ten to fifteen minutes. The nitride foils have a yellowish-bronze color.

Oxygen

Nickel foils can be oxidized in air in a furnace at about 700° C. to produce natural nickel oxide foils or in a closed system by means of an induction heater for monoisotopic oxygen. Nickel is used because of its ease of oxidation and the commercial availability of very thin foils.[1]

Carbon

Thick carbon targets, i.e. thicker than can be made from a carbon arc may be prepared by painting, spraying or dipping glass slides into Dag Dispersion #154[2], a colloidal graphite emulsion in isopropanol and floating off on water. They may be rendered oxygen-free by heating under vacuum to 1000° C for about one-half hour and cooling to room temperature in vacuum.

Calcium and Magnesium

Thin monisotopic targets of calcium and magnesium may be prepared by the reduction of the carbonate or oxide in a tantalum tube boat with an 1/8" diameter hole.

The temperature during initial heating is increased very slowly to degas the carbonate as it forms the oxide. The oxide is then reduced on the hot tantalum surface by the tantalum, but only for limited amounts of material, i.e. 50-150 mg. oxide. Typical target thickness is around 200 $\mu g/cm^2$. Thin nylon backings are used.

Rare Earth Oxides

Targets of enriched isotopes of the rare earth oxides are prepared by dropping a slurry in place.

A very dilute solution of polystyrene in benzene may be used instead of the water. The polystyrene binds the powder together and makes a much more rugged target.

Nylon films are prepared by dropping a hot dilute solution of nylon in isobutyl alcohol onto warm water. After ten to fifteen minutes a thin film can be picked up on a wire frame and mounted.

Lead and Bismuth

Lead and bismuth are evaporated from a tantalum boat at a temperature of about 700° C onto Zapon films backed by 100 mesh electromesh. The Zapon may be removed with amyl acetate.

The oxide coating on the metals is removed by momentarily evaporating at a higher temperature onto a shield convering the backing. After decreasing the temperature to approximately 700° C the shield is removed and evaporation continued onto the backing.

Zapon films are prepared by dropping Zapon Aequanite "A" lacquer[3] onto water, picking the film up on the electromesh and allowing it to dry thoroughly. (J. Sauer)

---

1 Nickel foils available from Chromium Corporation, Waterbury, Connecticut.
2 Available from Acheson Colloids Co., Port Huron, Michigan.
3 Available from Atlas Powder Co. Stamford, Connecticut or North Chicago, Illinois

---

X. APPENDIX

38. Statistics of Cyclotron Operation

The disposition of the time available for cyclotron operation during the period from May 16, 1963, to May 15, 1964, is given in Tables 38-1, 38-2, and 38-3.

Major loss of time was due to: 1) rebuilding of the main oscillator early in 1963, and 2) installing the new diffusion pump in the main vacuum system.

Table 38-1

Division of Cyclotron Time Among Activities

Activity	Hours	Percent
Normal Operation	4712	75.9
Setup of Experiments	296	4.8
Cyclotron Testing	138	2.1
Scheduled Repairs and Modifications	256	4.2
Unscheduled Repair	190	3.2
Failure of Experimental Equipment	47	.8
Unsatisfactory Cyclotron Operation	139	2.1
Unrequested Time	60	1.0
Visitors	15	.3
Total	6192	100.0

Table 38-2

Division of Normal Time Among Projectiles

Projectiles	Hours	Percent
Alpha Particles	3318	79.2
Protons	481	11.4
Deuterons	387	10.4
Total	4186	100.0

Table 38-3

Bombardments Performed for Outside Investigators

Investigator	Hours
Boeing Company	6.0
University of Oregon	7.0
Western Washington State College	15.0
Total	28.0

39. Cyclotron Personnel

Faculty

John S. Blair, Professor
David Bodansky, Professor
Arthur W. Fairhall, Professor
George W. Farwell, Professor
James B. Gerhart, Associate Professor
I. Halpern, Professor
Ksenofont Ilakovac, Visiting Associate Professor
Fred H. Schmidt, Professor
Robert Vandenbosch, Associate Professor

Cyclotron Research Staff

Jonas Alster, Research Assistant Professor
Ronald E. Brown, Research Assistant Professor
Charles D. Kavaloski, Research Assistant Professor
John S. Lilley, Research Assistant Professor
Ted. J. Morgan, Research Associate Professor:
Supervisor, Nuclear Physics Laboratory

Nelson Stein, Research Assistant Professor
Richard W. West, Research Instructor[1]
Claude F. Williamson, Research Assistant Professor

Predoctoral Associates

Chemistry

Walter Loveland

Physics

Joseph S. Heagney
David L. Hendrie
Wojciech Kolasinski
E. Roland Parkinson
Barry J. Shepherd
Gurnam S. Sidhu
Frederick W. Slee

Research Assistants

Chemistry

Charles J. Bishop
Derry D. Cooke
Robert L. Watters[2]

Physics

Wilfred J. Braithwaite
Nelson Cue
Robert Dickinson
Steve M. Ferguson[3]
Ramona P. Hammerly
Thomas D. Hayward
Paul Mizera
Roy J. Peterson
David C. Shreve
Derek W. Storm
Edward B. Warren

Full-Time Technical Staff

Machine Shop

Harvey E. Bennett, Foreman
Norman E. Gilbertson
Charles E. Hart
Floyd E. Helton
Gustav E. Johnson
Ed P. McArthur
Bernard Miller, Assistant Foreman
Byron A. Scott
Allen L. Willman

Electronic and Electrical

Laverne H. Dunning
Robert B. Elliott
Harold Fauska, Senior Physicist, Research Electronics Supervisor

Russell E. Karns
Carl E. Linder
George C. Monge
John W. Orth, Assistant Supervisor, Nuclear Physics Laboratory
George E. Saling
DeWayne L. Varnes
Norman G. Ward

Design and Drafting

Robert G. Clarke
Peggy Douglass
David W. Gough
Dolores Lenhart
Peter Momcilovich, Engineer
Lewis A. Page

Accelerator Operators

Barbara J. Barrett
Richard Clay[4]
Bonnie C. Murray
Georgia Jo Rohrbaugh

Others

Tylaine Hansen, Office Assistant
Kyum Ha Lee, Film Scanner
Diana Marshall, Secretary
Joanne M. Sauer, Radiochemist

Part-time Technical Staff

Student Helpers

Makoto Hori[3]
Kent McLean[3]
Carol Lewis Ming[3]
Tamae Sato[3]
Harry Winsor
Akiko Yamanouchi

Others

Mary A. Beard, Storekeeper
Joseph P. Knuehman, Storekeeper[3]
Don A. Miller, Storekeeper[3]
Patricia Woolf, Radiochemist[3]

---

1 Now at Rochester University, Rochester, New York.
2 Now at Atomics International Canoga Park, California
3 Terminated.
4 On military leave.

40. Advanced Degrees Granted, Academic Year 1963 - 1964

Robert Dickinson: M.S.
Edward B. Warren: M.S.
Robert L. Watters: Ph.D. A Radiochemical Study of the Helium-Ion Induced Fission of Pb^{206}.
Richard W. West: Ph.D. Proton Emission in 42-MeV Alpha Particle Bombardments of Several Elements.

41. List of Publications

"β Decay of C^{10} and the Cluster Model" Francis J. Bartis, Phys. Rev. 132, 1763 (1963).

"Experimental Evidence for Compound Nuclear Statistical Processes" D. Bodansky, Proceedings of the Conference on Direct Interactions and Nuclear Reaction Mechanisms (Padua, 1962), page 230; Gordon and Breach, 1963.

"Long Range Particle Emission in Coincidence with Fission at Moderate Excitation Energies" J. A. Coleman, A. W. Fairhall, and I. Halpern, Phys. Rev. 133, B724 (1964).

"Angular and Energy Distributions of Neutrons Emitted in Bombardments with 42 MeV Alpha Particles" D. M. Drake, P. Axel, and I. Halpern, Proceedings of the Conference on Direction Interactions and Nuclear Reaction Mechanisms (Padua, 1962), page 282; Gordon and Breach, 1963.

"Location of the 4^- Level in Zr^{90}" D. L. Hendrie and G. W. Farwell, Phys. Letters 9, 321 (1964).

"Proton Spin Flip and Substate Excitation in Inelastic Scattering" F. H. Schmidt, Ronald E. Brown, J. B. Gerhart, and W. A. Kolasinski, Nucl. Phys. 52, 353 (1964).